UNRAVELING THE FLUID-PRESENT METAMORPHISM OF SCHISTS FROM GARNET COMPOSITIONS IN THE BLACK HILLS, SOUTH DAKOTA

A Thesis presented to

the Faculty of the Graduate School

at the University of Missouri-Columbia

In Partial Fulfillment

of the Requirements for the Degree

Master of Science

---

by

Yanying Chen

Dr. Peter I. Nabelek, Thesis Supervisor

JULY 2012

The undersigned, appointed by the dean of the Graduate School, have examined the thesis entitled

UNRAVELING THE FLUID-PRESENT METAMORPHISM OF SCHISTS FROM GARNET COMPOSITIONS IN THE BLACK HILLS, SOUTH DAKOTA

presented by Yanying Chen,

a candidate for the degree of Master of Science,

and hereby certify that, in their opinion, it is worthy of acceptance.

Dr. Peter I. Nabelek

Dr. Robert L. Bauer

Dr. Angela Speck

ACKNOWLEDGEMENTS

It is a pleasure to thank those who made this thesis possible. First of all, I would like to show my deepest gratitude to my advisor Dr. Peter Nabelek who provided me the opportunity to participate in this project. His guidance, encouragement and support from the initial to the final level are highly appreciated. He is always patient with all my questions and offers helpful advices. It is a comfortable and pleasant experience to work with him. Without him, I would not be able to have come this far.

I would like to thank my committee members, Dr. Bob Baurer and Dr. Angela Speck for their assistance and suggestions for improving my thesis. Thank you to all my teachers, Alan Whittington, Mian Liu, Martin Appold and Louis Ross, who instructed me in professional knowledge and gave me a lot of help during and after class time. Thank you to Paul Carpenter at Washington University, St. Louis, for his assistance during my lab visits. Also thank you to my colleagues for company and fun in the past two years.

I would like to thank my parents who always have been my powerful backing. Their trust and endless love make me never afraid of any challenges and difficulties. Many thanks to my friends Kim Boley, Lingfei Yan, Hongyu Fan, Amber Farhat and Amanda Summers, who are always there with me.

Last but definitely not least, thank you to the National Science Foundation for its generous funding of this project.

TABLE OF CONTENTS

LIST OF FIGURES

Figure **Page**

LIST OF TABLES

Table **Page**

ABSTRACT

Garnets in Proterozoic metapelites in the Black Hills, South Dakota, were analyzed to determine their pressure, temperature and hydrothermal conditions of growth and to elucidate pressure-temperature-time (P-T-t) paths of their host rocks. The metapelites are the product of garnet-grade regional metamorphism beginning at ~1755 Ma due to the collision of Wyoming and Superior cratons and subsequent contact metamorphism by intrusion of the Harney Peak Granite (HPG) at ~1715 Ma. Garnet occurs in the garnet zone, and contact-metamorphic staurolite and sillimanite zones. X-ray element maps and compositional profiles across garnets were determined using electron-probe microanalysis (EPMA). Mineral assemblage diagrams (pseudosections) with garnet composition contours were constructed using the THERIAK-DOMINO software. The diagrams provide a foundation for determining the conditions of garnet growth and P-T-t paths for their host rocks.

In the garnet zone, garnets have inclusion-rich centers and almost inclusion-free rims. The garnets display low-Ca cores (X_{grs} = 0.08-0.1), followed by slightly more elevated Ca annuli (X_{grs} ~ 0.1) and low-Ca rims (X_{grs}<0.1). Fe increases from core (X_{alm} ~ 0.4-0.5) to rim (X_{alm} ~ 0.5-0.7). Mn decreases from core (X_{sps} ~0.38-0.45) to rim (X_{sps} ~ 0.3-0.4). Mg slightly increases from X_{py} < 0.05 in cores toward rims. Y concentrations are higher in cores and some garnets display high-Y annuli near or at rims. From cores toward rims, indicated pressure increases nearly isothermally and gradually from ~2.4 to ~4.5 kbar. The very rims show slightly more elevated temperatures by ~30^{o}C. The rims potentially indicate a late heating pulse due to regional leucogranite magmatism.

In the staurolite zone, garnets contain fewer inclusions. Zoned garnets have relatively high-Ca cores (X_{grs}~0.1) and low-Ca rims (X_{grs} ~0.03). Fe increases from cores (X_{alm} ~ 0.5) to rims (X_{alm} ~ 0.82), Mn decreases from cores (X_{sps} ~0.21-0.35) to rims (X_{sps} ~0.08) and Mg increases from cores (X_{py} ~0.04) to rims (X_{py}~0.1). Y displays high concentrations in cores and some garnets also have high-Y annuli. Indicated pressures during growth of cores are 3 to 3.5 kbar whereas rims indicate pressures of 4 kbar. From cores to rims, temperature increased from ~500 ^{o}C to more than 600^{o}C.

In the sillimanite zone, garnet zoning is minimal. X_{grs} is <0.05 and X_{alm} ~ 0.77. Mn is uniform (X_{sps}~0.1) except for slightly elevated concentrations in rims. X_{py} is <0.1, except in rims where it is lower. Y concentrations are high in the cores. From core to rim, indicated pressure decreases from >5 kbar to ~4.2 kbar.

The geochemical characteristics of the garnets and the derived P-T-t paths were used to determine the cause of zoning and the dynamo-thermal metamorphic history of the Proterozoic core of the Black Hills. Calculations show that internal chemical diffusion would have been too slow for modification of garnet chemistry after crystallization. Thus, the chemical zoning must reflect conditions during garnet growth. In the garnet and staurolite zones, garnets initially grew in a low a(H_2O) environment and the temperature of initial growth may have overstepped the equilibrium temperature. In the sillimanite zone, low-grade garnet partially or fully recrystallized in a higher a(H_2O) environment and compositions suggest equilibrium growth commensurate with sillimanite-grade temperatures. Garnet compositions suggest that the early regional metamorphism occurred at relatively low pressures (~3 kbar), whereas the region in close proximity to the HPG had a high-P history (>6 kbar) that is supported by an occurrence of kyanite in one sillimanite-zone sample.

Introduction

Minerals in the garnet group occur in various types of metamorphic rocks and are stable over a wide range of temperature and pressure conditions due to the framework of tetrahedrally coordinated Si, octahedrally coordinated 3^+ cation sites and eight-fold coordinated 2^+ cation sites (Deer et al., 1992). Chemical zoning is typical in garnets and it can be used to decipher the metamorphic conditions during garnet crystallization. Element maps of garnets can reveal in detail the changing conditions of garnet growth. Zoning can arise from different factors that depend on the local or regional geologic history, including elemental fractionation during growth, fluid composition, the breakdown or growth of other minerals in host rocks, and diffusion (e.g. Cygan and Lasaga, 1982; Anderson and Buckley, 1973; Hickmott and Spear, 1992; Hickmot et al., 1987). Thus, origins of garnet zoning can be multiple and superimposed, so that zoning can implicate a variety of metamorphic conditions associated with metamorphic events. Advanced geochemical analytical instruments, such as the electron microprobe that produces X-ray zoning maps for different components of minerals, enable detailed analysis of garnets from which conditions of metamorphism can be determined. The purpose of this study is two-fold: 1) to evaluate the causes of garnet zoning in Black Hills garnet, and 2) to determine pressure-temperature-time (P-T-t) paths for the examined regions of the Proterozoic core of the Black Hills.

Garnets nucleate and grow at different periods of metamorphism, depending on what elements are provided by the matrix and mineral reactions. Fractionation

mechanism of major elements and trace elements may be different, depending on the prevailing equilibrium constants. With changes in temperature and pressure, diffusion may also influence garnet zoning. Spear and Daniel (2001), based on their research in Harpswell Neck, Maine, USA, proposed that Ca zoning in garnet was diffusion controlled, whereas Fe, Mg, and Mn zoning reflects evolving equilibrium with the rock matrix. Spear and Kohn's (1996) research near Fall Mountain, New Hampshire, USA, points out that zoning of trace elements, including Sc, Y, P and Cr, is not easily modified by diffusion. Zoning of these elements in Fall Mountain garnets is discontinuous and correlates with fluid-absent melting of the host rocks. Y may be released from garnet by diffusion at high temperatures to promote the growth of monazite in the absence of xenotime (Spear and Pyle, 2010). Daniel and Spear (1998) suggested that garnets can grow by coalescence of multiple nuclei that thereafter grow as a continuous advancing rim and MnO contours in those garnets can serve as a proxy for patterns of garnet nucleation and growth.

Carlson (2002) suggested that different elements in garnets equilibrate at different scales due to the sluggishness of intergranular diffusion. Research by Meth and Carlson (2005) in Passo de Sole, Switzerland, shows that even during syn-kinematic crystallization, intergranular diffusion rates governed garnet nucleation, growth and chemical zoning. They suggested that Ca zoning was affected by an influx of a Ca-bearing fluid. Mn zoning shows disequilibrium during the early stage of garnet growth, whereas Fe and Mg were in equilibrium with the matrix, with zoning of these elements compensating for disequilibrium Ca and Mn zoning. Thus, potential fluid influx and fluid composition cannot be ignored as a control on garnet growth. H_2O activity was also

thought to affect the rate of intergranular diffusion in the Makhavinekh Lake Pluton, northern Labrador, Canada (Carlson, 2010).

Previous studies of garnet in metapelites in the Black Hills, South Dakota, showed that it is an excellent mineral for unraveling the Proterozoic metamorphic history of the region. Schwandt et al. (1996b) showed that major and trace element zoning in garnet is more pronounced in lower metamorphic grades than in higher grades. Major element zoning does not appear to be related to volume-diffusion. Trace element (REE, Cr, Ti, V, Y, Zr) zoning was attributed to fractionation mechanisms, limited intergranular diffusion and variations in partition coefficients. However, an influence of variable fluid composition was not considered as a possible factor in controlling zoning. A key concept, that fluids may induce wholesale recrystallization of garnet at high metamorphic temperatures, was proposed by Nabelek et al. (2006). Because Fe-rich garnet is more stable at high metamorphic grades than Mn-rich garnet, a mechanism of reequilibration may be dissolution of an old Mn-rich garnet and reprecipitation of a new Fe-rich garnet. Variations of fluid compositions at different metamorphic grades reinforced the idea that low activity of H_2O is essential for preservation of zoning in garnet (Huff and Nabelek, 2006).

In this study, new X-ray chemical maps and zoning profiles across garnets in the different metamorphic zones in the Black Hills were determined by electron-probe microanalysis (EPMA). Based on this analysis, garnet zoning of the major and some trace elements in the different metamorphic zones is illustrated. The zoning patterns have implications for the conditions under which the garnet grew and reequilibrated in response to chances in temperature, pressure, and fluid composition. By combining the

quantitative data with pseudosections showing mineral assemblages and garnet composition contours, constructed using a thermodynamic database, the pressure and temperature (P-T) history of the Black Hills can be unraveled.

Geologic Background

Metamorphic history

Proterozoic metamorphic rocks in the Black Hills were partly exposed by late-Mesozoic to early-Tertiary Laramide uplift and erosion (Redden et al. 1990). The metamorphic rocks were formed mainly by a polyphase deformational history, including a regional thrusting event and metamorphism related to Yavapai arc accretion from the south (Dahl et al. 1999). Metamorphism and deformation that dominates the core of the Black Hills is related to the collision of the Wyoming and Superior cratons (Terry and Friberg, 1990; Redden et al., 1990) and a subsequent contact metamorphism and deformation superimposed in the regional metamorphism by intrusion of the Harney Peak Granite (Helms and Labotka, 1991; Nabelek et al., 2006).

The earlier higher-grade metamorphism (M_1), as indicated by occurrence of kyanite, was restricted to the Bear Mountain area on the western margin of the Precambrian core of the Black Hills (Figure 1). It was caused by deformation (D_1) that took place in the deeper crust between about 1790 and 1750 Ma and resulted in producing foliation S_1 (Dahl et al, 2005a, b). It was demonstrated by a P-T-t path for the Bear Mountain Dome (Figure 2; Terry and Friberg, 1990; Dahl et al. 2005b).

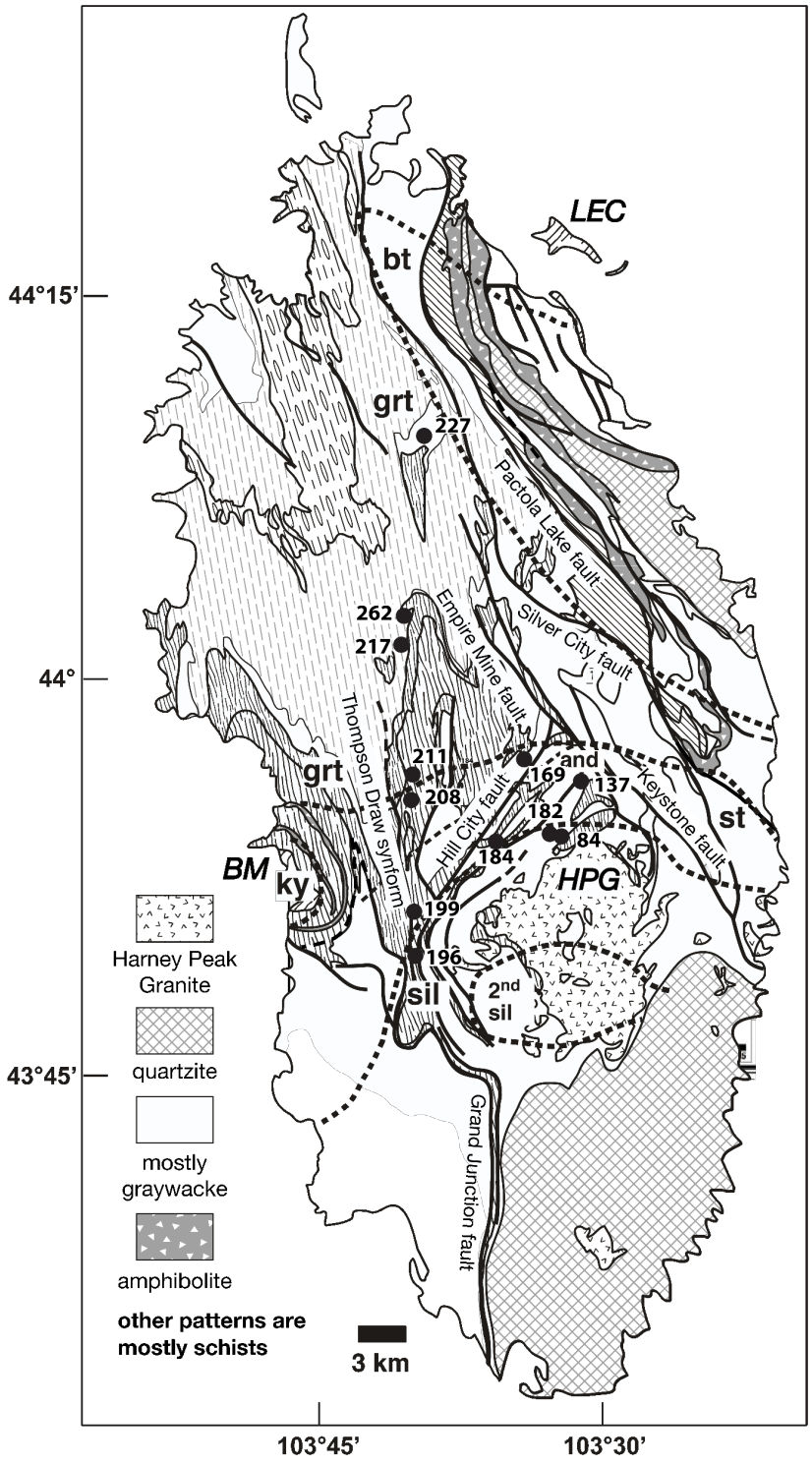

Figure 1 Geological map of the Black Hills. Light solid lines: formation boundaries; heavy solid lines: faults; dashed lines: metamorphic isograds; black dots and numbers: sample locations and their numbers. BM: Bear Mountain; LEC: Little Elk Creek. Modified after DeWitt et al. 1986, 1989; Helms and Labotka, 1991; Nabelek et al. 2006; Redden and DeWitt, 2008.

The largely low-grade regional metamorphism (M_2) accompanying deformation (D_2) and producing foliations (S_2) influenced most of the Black Hills core (Redden et al., 1990; Terry and Friberg, 1990). The deformation and metamorphism were the products of E-W shortening caused by the collision of Wyoming and Superior cratons beginning at 1750±10 Ma (Dahl et al, 2005a, b).

Contact metamorphism (M_3) occurred in response to emplacement of the Harney Peak Granite (HPG) at 1715±10 Ma (Krogstad and Walker, 1994; Redden et al., 1990;). It caused the production of foliation S_3 that is often concordant with the granite sills that make up the HPG. The foliation is attributed to the distention of country rock during multiple intrusions of granite melt (Duke et al. 1988). The M_2 and M_3 metamorphic events probably overlapped since they occurred in a relatively short space of time (Redden and DeWitt, 2008).

Fluids were present during both the regional M_2 metamorphism and contact metamorphism. Fluids during regional metamorphism, that reached at least the garnet grade, mainly contained CH_4 or CO_2 and N_2, based on analysis of fluid inclusions in quartz veins (Huff and Nabelek, 2007). Fluids occurring during contact metamorphism near the HPG were dominated by H_2O with <20% CO_2 and fluid flow caused metasomatism by alkali (Na, K, Li) and B-rich fluids emanating from the crystallizing granite melts (Redden and Norton, 1992; Duke, 1995, 1996; Wilke et al., 2002; Nabelek et al, 1993, 2003, 2006; Huff and Nabelek, 2007).

Mineral assemblages

In this thesis, garnets related to the regional M_2 metamorphism and the following M_3 contact metamorphism were examined. The regional garnet zone was later superimposed upon by heat and fluids emanating from the HPG intrusion. Metamorphic isograds (Figure 1) are distributed over a distance of 10 km to 15 km, including garnet, staurolite, sillimanite, and sillimanite + K feldspar isograds (Helms and Labotka, 1991; Nabelek et al., 2006; Redden and DeWitt, 2008). The isograds divide the Precambrian metamorphic region into the biotite zone, garnet zone, staurolite zone, sillimanite zone and the second-sillimanite zone. Major mineral assemblages are different for each zone but garnet, staurolite and sillimanite zones contain the same accessory minerals, including ilmenite, tourmaline, monazite and zircon (Schwandt et al. 1996b). Research in this thesis is related to the garnet, staurolite and sillimanite zones.

Garnet zone

The garnet isograd generally follows the Silver City fault from the eastern Black Hills to the northern Black Hills (Helms and Laboka, 1991; Nabelek et al., 2006). It was defined by the first appearance of garnet or chlorite-bearing pseudomorphs after garnet. In the north, the isograd begins to trend southeastwardly, due to the likely presence of a buried granite near Crook Mountain, a granite similar to the HPG that was identified in cores drilled by the Homestake Mining Company (Redden and DeWitt, 2008). It was dated at 1.68 Ga. The garnet zone includes the lower garnet zone and the upper garnet zone, but their boundary is diffuse (Nabelek et al. 2006). The upper garnet zone is characterized by garnet grains that have inclusion-free overgrowths and by the occurrence of chlorite that overgrowths the regional foliation, both of which were

attributed to influence of contact metamorphism (Nabelek et al. 2006). MnO concentrations are generally higher in garnets in the lower garnet zone (Stone, 2005; Nabelek et al., 2006). Trace elements throughout the garnet zone have higher concentration in cores of garnets compared to rims (Schwandt et al. 1996b).

Staurolite zone

The staurolite zone is located in the central part of the Black Hills (Figure 1). Near the staurolite isograd, the original regional foliation persists but there are modifications by later mineral crystallization (Redden and DeWitt, 2008). Chlorite grains were found to grow across the regional foliation. The chlorite indicates fluid flow during contact metamorphism (Nabelek et al. 2006). Other areas in the staurolite zone developed a younger schistosity related to the HPG intrusion (Redden and DeWitt, 2008). Staurolite formed by consumption of the chlorite by reaction

$$chl + grt + ms \rightarrow st + bt + qtz + H_2O \quad [1]$$

(Nabelek et al. 2006). The staurolite zone contains two types of garnet. Old inclusion-rich garnet crystals that have inclusion-free overgrowth occur in the Thompson Draw synform (Friberg et al. 1996). New inclusion-poor garnets, that probably grew by recrystallization of the older, inclusion-rich garnets in a fluid rich environment, mainly occur north of the Harney Peak Granite as well as in its western aureole (Nabelek et al. 2006). Most staurolites overgrow the regional foliation. Some staurolites later reacted to muscovite + biotite due to influx of K-bearing aqueous fluids. Because S_3 foliation wraps around the pseudomorphs after staurolite but the replacement micas are not foliated shows that deformation postdated growth of some staurolites but preceded the staurolite replacement.

Sillimanite zone

Sillimanite formed by the reaction

$$st + ms + qtz \rightarrow sil + grt + bt + H_2O \quad [2]$$

(Nabelek et al. 2006). Sillimanite grains are fibrolitic. Regional foliation in the sillimanite zone was rotated and flattened by HPG intrusion (Hill et al. 2004). Rocks are less graphitic than at lower grades and contain inclusion poor and unzoned garnet grains (Nabelek et al. 2006).

Although the metamorphism in the Black Hills has previously been described as a high temperature/low pressure type (e.g. Helms and Labotka, 1991), kyanite was identified in sample 182 (Figure 1) located to the north of the HPG near the sillimanite isograd. The kyanite indicates a high-pressure history of the high-grade aureole of the HPG.

Second-sillimanite zone

Garnet is almost absent in second sillimanite zone (Nabelek et al., 2006). Muscovite breakdown to K-feldspar occurred in this zone. It was accompanied by partial melting that formed migmatites with the assemblage of biotite + sillimanite + quartz + plagioclase + tourmaline + poikioblastic K-feldspar (Shearer et al. 1987; Nabelek 1997, 1999; Nabelek et al. 2006). Sillimanite in this zone grew prior to the completion of granite intrusive activity (Redden and DeWitt, 2008). Lack of garnet in this zone is perhaps due to the presence of tourmaline in granite leucosomes that consumed Fe that would be necessary to stabilize garnet.

Retrograde andalusite zone

Helms and Labotka (1991) identified an andalusite (± cordierite) zone based on the occurrence of andalusite (Figure 1). They located an andalusite isograd between the staurolite and sillimanite isograds. However, the occurrence of andalusite suggests that it is mostly a retrograde mineral that grew upon decompression in the presence of a low a(H_2O) fluid (Nabelek et al., 2006). Andalusite mostly grew along foliations close to shear zones and faults, and generally it occurs as a poikioblastic mineral. It also occurs together with quartz and graphite in veins in the high-grade part of the aureole of the HPG. Prograde growth of andalusite is also inconsistent with the pressure of prograde contact metamorphism that was >4 kbar (Nabelek et al., 2006; this thesis).

P-T-t history in the Black Hills

A pressure-temperature-time path for the Bear Mountain Dome area on the western margin of the Black Hills' core (Figure 2) was constructed by Dahl et al. (2005b) by synthesizing microstructure, petrology and microchronometry (Terry and Friberg, 1990; DeYoreo et al., 1991; Williams and Karlstrom, 1996; Holm et al., 1997; Dahl and Frei 1998). Two clockwise P-T-t paths are suggested that respectively represent conductive and/or shear heating of metasediments related to burial of sediments to the mid-lower crust (D_1) at ~1775-1750 Ma and then deeper during (M_2) until reheating occurred during emplacement of the Harney Peak Granite (M_3) at ~1715 Ma to 1690 Ma (Redden et al. 1990; Holm et al. 1997; Dahl et al. 2005b). However, unique P-T-t paths, as shown in Figure 2, cannot be constructed for all of the Black Hills. For example, P-T paths of garnets in part of the staurolite zone were calculated by program GIBBS

showing an almost isobaric heating during garnet growth (Nabelek et al. 2006). Temperatures calculated by the garnet-biotite Fe-Mg exchange thermobarometer using THERMOCALC (Nabelek et al. 2006) display a temperature rise from the northern Black Hills towards the HPG. Temperature distributions correspond to different metamorphic isograds and zones. Temperatures close to the garnet isograd are < 430^{o}C. Temperatures on north side of the staurolite isograd are < 480^{o}C and on south side of the staurolite isograd are > 480^{o}C. Temperatures are mostly ~550^{o}C around sillimanite isograd and > 590^{o}C in second sillimanite zone. They are lower than the calculated temperature in a pseudosection might be because of the low H_2O activity in fluid that influenced the stability field of garnet (Nabelek et al. 2006). A block that included the HPG and a region between the Hill City and Keystone faults was apparently uplifted during magma intrusion (Nabelek et al. 2006). It is consistent with the noted kyanite occurrence to the north of HPG.

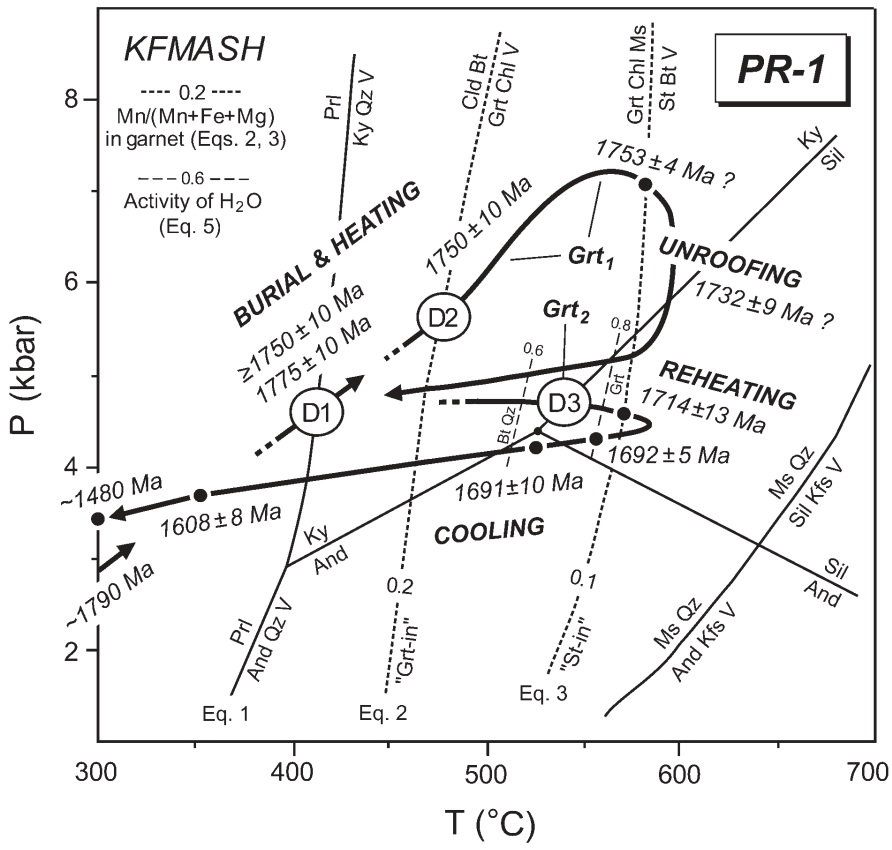

Figure 2 P-T-D-t paths with petrogenetic grid reconstructed by Dahl et al. (2005b) for the Bear Mountain dome. Modified after Terry and Fiberg (1990); Holm et al. (1997); Dahl and Frei (1998) and Spear et al. (1999). And: andalusite; Ky: kyanite; Sil: sillimanite; Bt = biotite; Chl = chlorite; Cld = chloritoid; Grt = garnet; Kfs = K-feldspar; Ms = muscovite; Prl = pyrophyllite; Qz = quartz; St = staurolite; V = vapor (H_2O). Dashed H_2O activity isopleths were calculated by TWEEQU (Ver. 2.02; Berman 1991).

Methods

Sample preparation

Twenty-two garnets from eleven samples representing all garnet-bearing zones were analyzed. Samples were gathered previously by Dr. Peter Nabelek and co-workers. The samples were cut into billets by a diamond saw and were sent for standard, polished, thin-section preparation. Prior to EPMA, thinsections were coated with carbon to make them electrically conductive.

Garnets representing the range of observed metamorphic zones and textures were selected for EPMA by X-ray mapping and detailed spot profiles. Some garnets were pre-scanned using Scanning Electron Microscopy (SEM), including for approximate zoning of major elements, rough inclusion identification, and growth morphologies. The selected samples, 227-1, 262-1, 262-2, 217-1 and 211-1 are from the garnet zone; samples 208-2, 169-3, 137-1, 184-1 and 199-1 are from the staurolite zone, and samples 196-4 and 84-1 are from the sillimanite zone. Some of these samples were previously examined by Nabelek et al (2006).

Microprobe analysis

Samples were bombarded with an electron beam and emitted backscatter electrons (BSE) and X-rays at characteristic wavelengths for examined elements. BSE images were collected in order to examine the spatial relationships of garnet and adjacent phases as well as mass-dependent zoning and inclusions within the garnets. X-ray map acquisitions

were done by wavelength dispersive spectrometers (WDS) for several hours. X-ray intensity maps for 12 elements, including Fe, Mg, Mn, Ca, Y, Ti, Si, Al, Zr, Cr, K and Na, were produced at 15 kV accelerating voltage and 100 nA beam current. The pixel size and dwell time were slightly different for each garnet, but dwell times ranged from 60 ms to 130 ms. The X-ray maps were then colored and scaled by the National Institutes of Health program IMAGE-J.

Nine samples were selected for further quantitative zoning profiles. 15 kV accelerating voltage and 25 nA beam currents were used with beam size 10μm. For each analyzed garnet, about 20-point traverses were made.

Petrography

Microscopic observations of metapelites provide visual assessment of garnet growth and its environment at each metamorphic grade. Moreover, fluid flow evidence and some kinetic and reaction relationships can be identified. Garnet has variable size throughout the Black Hills. Most grains are around 700 μm in the lower garnet zone, although in sample 211-1 garnet is larger (~750 μm to ~1500 μm). In the staurolite zone, garnets in samples coming from the area between the Hill City Fault and the Keystone Fault are larger than garnets on the far sides of the faults. Garnets in the sillimanite zone are smaller (~200 μm to 500 μm) than in most samples in the staurolite zone.

Garnet zone

Metapelites in the lower garnet zone are very graphitic. Sample 227-1 in lower garnet zone contains the mineral assemblage of garnet + biotite + muscovite + quartz + plagioclase. Garnet grains occur as euhedral or subhedral porphyroblasts grown post-kinematically and contain many graphite inclusions. Some of the garnet grains display radial crystallization patterns that potentially indicate a chemical disequilibrium condition during rapid garnet growth (Wilbur and Ague, 2006) (Figure 3a).

Samples 262-1 262-2 and 217-1, obtained between the Thompson Draw synform and the Empire Mine fault, also have a porphyroblastic texture with mineral assemblage of garnet + muscovite + biotite + quartz + plagioclase. Garnet grains are porphyroblasts that crystallized post-kinematically. They have large graphitic cores with or without

radial texture (Figure 3b, d). Garnets mostly grew in graphitic bands (Figure 3c, d), but extremely graphitic bands (Figure 3c) contain fewer garnet grains than less graphitic bands (Figure 3d).

Sample 211-1 comes from the upper garnet zone from near the staurolite isograd, also near the Thompson Draw synform. It has the mineral assemblage garnet + biotite + muscovite + quartz + chlorite. Garnet porphyroblasts grew in five different bands with distinct features. The first band is severely graphitic and contains garnet grains that grew pre-kinematically with large and branched inclusion-rich cores and inclusion-free rims (Figure 3e). The second band, that is less graphitic than the first band, has garnet porphyroblasts with large inclusion-rich cores and inclusion-free overgrowths (Figure 3e). The garnets also appear to be pre-kinematic. Quartz-rich veins occupy a large proportion of the third band (Figure 3f). Garnet grains are elongated and grew along layers with recrystallizated biotite, suggesting that the garnets grew in the presence of an aqueous fluid. The fourth band (Figure 3g) contains larger garnets with large inclusion-rich cores and inclusion-free overgrowth. Inclusions in the crystals display radial distributions located between sectors of garnet grains. A few post-kinematic chlorite crystals that grew across foliation occur in this band. They are attributed to fluid infiltration during intrusion of the HPG. The fifth band appears similar to the second one with garnet grains that have inclusion-rich cores and inclusion-free rims. However, the garnets are pre-kinematic to syn-kinematic (Figure 3h). This band also includes recrystallized biotite and quartz and post-kinematic chlorite grains. Some apparent quartz veinlets have oblique orientations from foliation. They also indicate a fluid-rich condition.

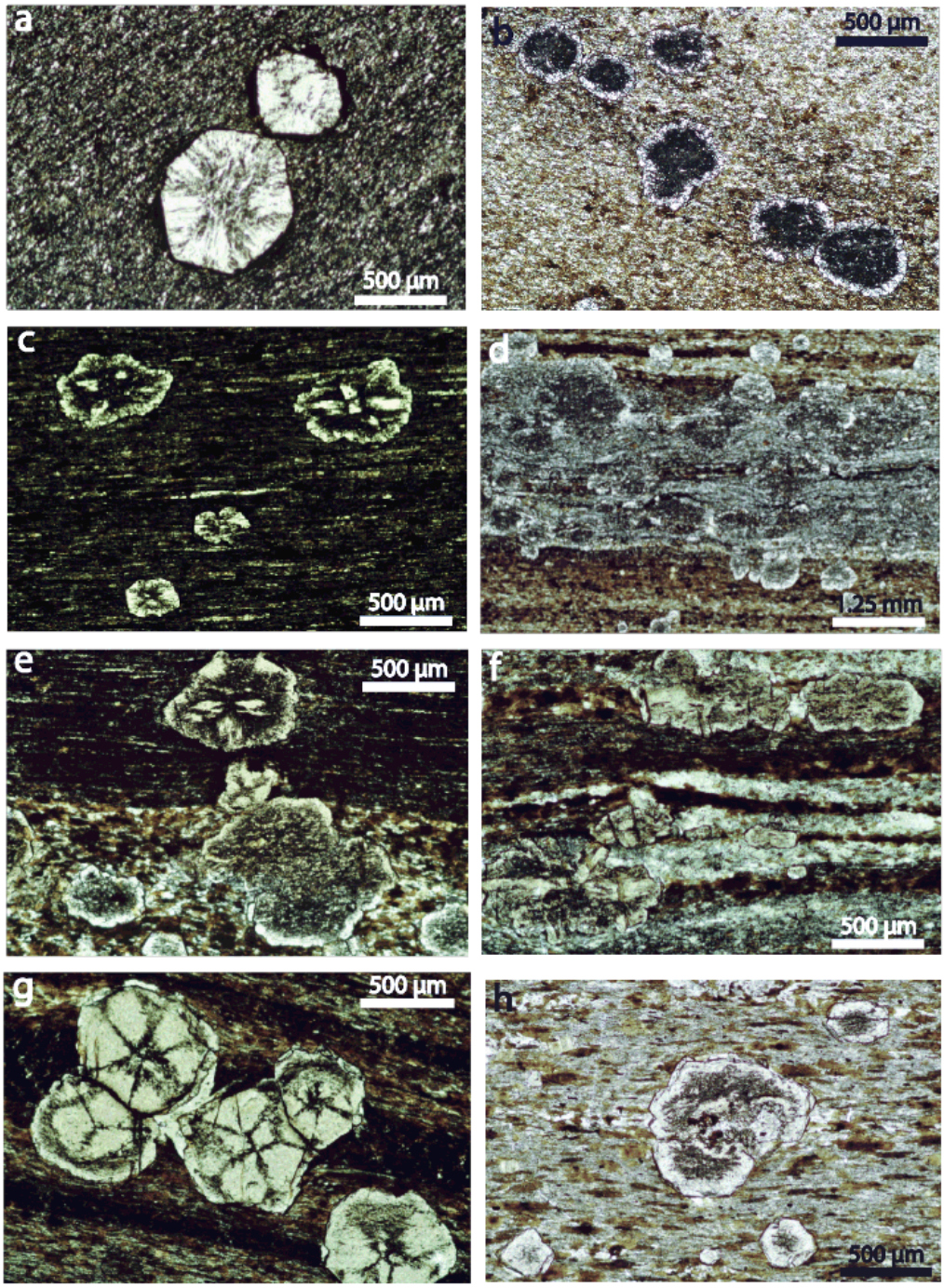

Figure 3 Petrographic characteristics of garnets in the garnet zone. Garnets prefer to grow in graphtic bands with inclusion-rich core and inclusion-poor rim. a. Garnet crystallization in radial patterns with many graphite inclusions between branched parts in sample 227-1; b. garnet has a large inclusion-rich core and an inclusion-free rim in sample 262-2; c. Garnets with branched cores in extremely graphitic bands in sample 262-1; d. More garnets grew along graphitic bands in sample 262-1; e. Two different bands have different morphologies of garnet in sample 211-1; f. Garnet between quartz veins in sample 211-1; g. garnet with radially distributed inclusions in sample 211-1; h. Syn-kinematictic garnet with spiral crystallization in sample 211-1.

Staurolite zone

Samples 208-2 and 169-3, collected near the staurolite isograd, have mineral assemblage of garnet + biotite + muscovite + quartz + chlorite + plagioclase. Some garnet grains are anhedral to subhedral with only few inclusions (Figure 4a), but some grains have inclusion-rich cores, similar to grains in the garnet zone. Recrystallized biotite and cross-foliation chlorite are attributed to fluid influx (Figure 4b).

Samples 137-1 and 184-1 were collected in an area between the Hill City fault and the Keystone fault. In this area, the S_2 foliation was transposed to a more horizontal orientation during emplacement of the HPG. The samples contain the assemblage garnet + staurolite + biotite + muscovite + quartz + plagioclase. Garnet and staurolite are porphyroblasts. Garnet in sample 137-1 is almost inclusions-free and euhedral to subhedral (Figure 4c). Apparently, older and low-grade garnet grains were consumed and recrystallized to new garnets (Nabelek et al. 2006). Staurolite is euhedral and has many quartz and other inclusions. Evident recrystallization of biotite may have led to some disturbance of the regional foliation. Sample 184-1, which was collected closer to the sillimanite isograd, contains larger garnets and more staurolite crystals. Garnets appear to be pre-kinematic and most are subhedral (Figure 4d). Staurolite is post-kinematic with many quartz inclusions. The matrix displays strong foliation formed by biotite and there is an apparent increase in grain size of quartz.

Sample 199-1 comes from close proximity to the Thompson Draw synform. It has an assemblage of garnet + biotite + muscovite + quartz + plagioclase + chlorite. Garnet grains are porphyroblasts. They contain large, inclusion-rich cores with graphite, chlorite,

quartz and biotite inclusions and narrow, inclusion-poor rims (Figure 4e). They appear to be pre-kinematic. Recrystallized biotite and quartz in the matrix suggest fluid infiltration.

Sillimanite zone

Sample 196-4 taken from the Thompson Draw synform has the mineral assemblage biotite + garnet + quartz + plagioclase + chlorite. Garnets are euhedral to subhedral. Some of the garnet grains are not fully recrystallized and retain characteristics of lower-grade garnet grains before recrystallization. Some grains were partially retrograded into chlorite (Figure 4f). The sample contains smaller, inclusion-free garnets that may have resulted from the breakdown of old ones (Figure 4g). Post-kinematic chlorite may be the product of alteration of garnet and/or biotite.

Sample 84-1 from north of the Harney Peak Granite has the mineral assemblage of garnet + biotite + sillimanite + muscovite + quartz. It is representative of pelites in this high-grade part of the aureole. Garnet and sillimanite are porphyroblasts. The sample, including garnets, is generally devoid of graphite. Garnet grains are anhedral to euhedral, mostly pre-kinematic, and with few inclusions. Sillimanite has the fibrolite form and is pre-kinematic to syn-kinematic (Figure 4h).

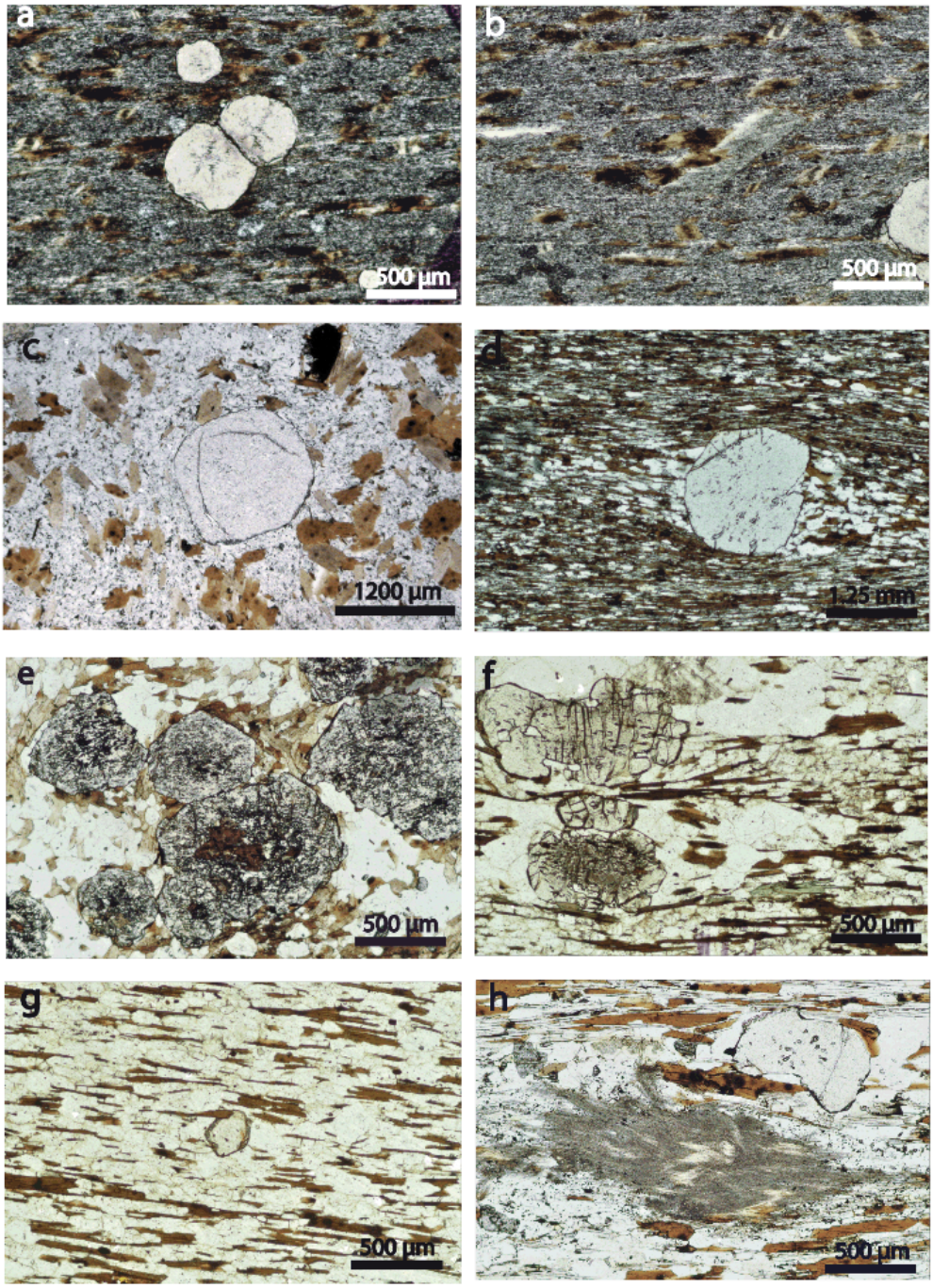

Figure 4 Petrographic characteristics for garnets in staurolite and sillimanite zones. a. Garnet grains are almost inclusion-free in sample 208-2. b. Chlorite grew across the foliation. c. Euhedral garnet in sample 137-1. d. Euhedral garnet in sample 184-1 with fluid mediated foliations. e. Garnets contain large biotite inclusions in sample 199-1. f. Partially recrystallizated garnet in sample 196-4 and chlorite grew along foliations. g. Small, new garnet in sample 196-4. h. Garnet and sillimanite porphyroblasts in sample 84-1.

X-ray element maps

Garnet zone

In the garnet zone, garnets have inclusion-rich centers, which are relatively dark in BSE images, and almost inclusion-free dodecahedral overgrowths. All garnets in the zone display low-Ca cores (Figure 5) and Ca concentrations increase toward rims, with a particularly sharp increase in the dodecahedral overgrowths. The very rims of garnets in samples 262-2 and 211-1 have again lower Ca concentrations (Figure 5). Ca zoning is correlated with bright and dark portions of BSE images of sample 211-1. The bright portions have low-Ca concentrations and the darker portions have high-Ca concentrations. The radially distributed inclusions are Ca-rich. They may indicate a past presence of calcite in the graphitic bands where garnet grew (Figure 3g). Mn generally decreases from cores toward rims of all garnets, Mg is elevated in the rims, and Fe concentrations are also slightly elevated at the rims.

Most X-ray maps display high-Y cores that have fairly sharp boundaries. Garnets in samples 227-1, 262-2 also show high-Y annuli near rims that mark dodecahedral overgrowths (Figure 5). The high Y cores suggest that the graphitic layers in which the garnets nucleated contained high Y concentrations, perhaps in the form of an yttrium phosphate mineral such as xenotime.

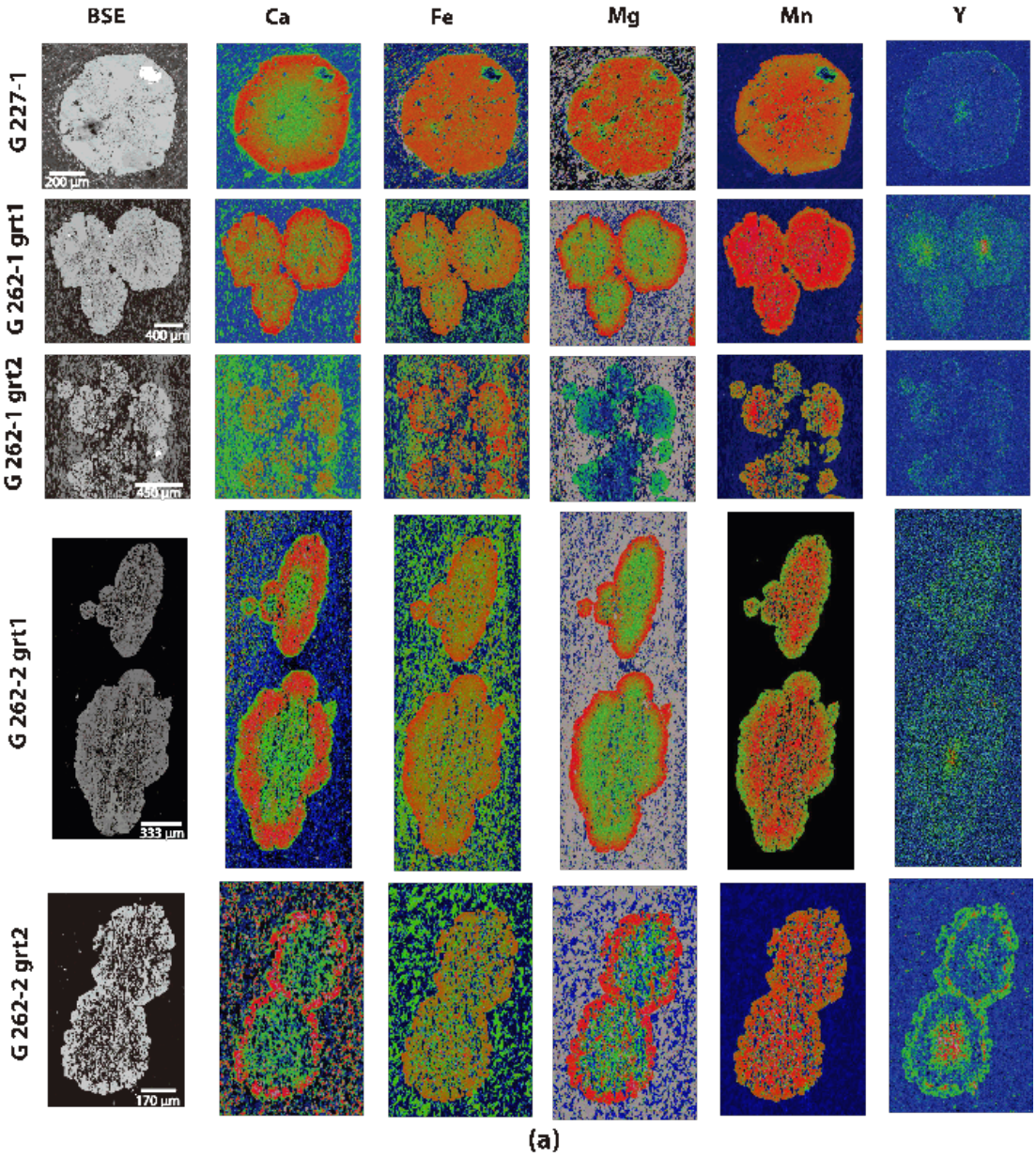

Figure 5 X-ray zoning maps of Ca, Fe, Mg, Mn and Y. Sample 227-1, 262-1, 262-2, 217-1 and 211-1 are from the garnet zone. Sample 208-2, 169-3, 137-1,184-1 and 199-1 are from the staurolite zone. The sillimanite zone contains Sample 196-4 and 84-1. Ca concentrations are low in the cores in the garnet zone but high in the cores in the staurolite zone and the sillimanite zone. High-Fe rims exist at low grade except in garnet in sample 227-1 and Fe zonings become uniform at high grade. Mg concentrations are generally higher in the rims in low grades. At high grades, Mg displays low-Mg rims on garnet grains. Mn has higher concentrations in the cores in the garnet zone and most samples in the staurolite zone but high-Mn rims occur at high grade. Most samples have high-Y cores.

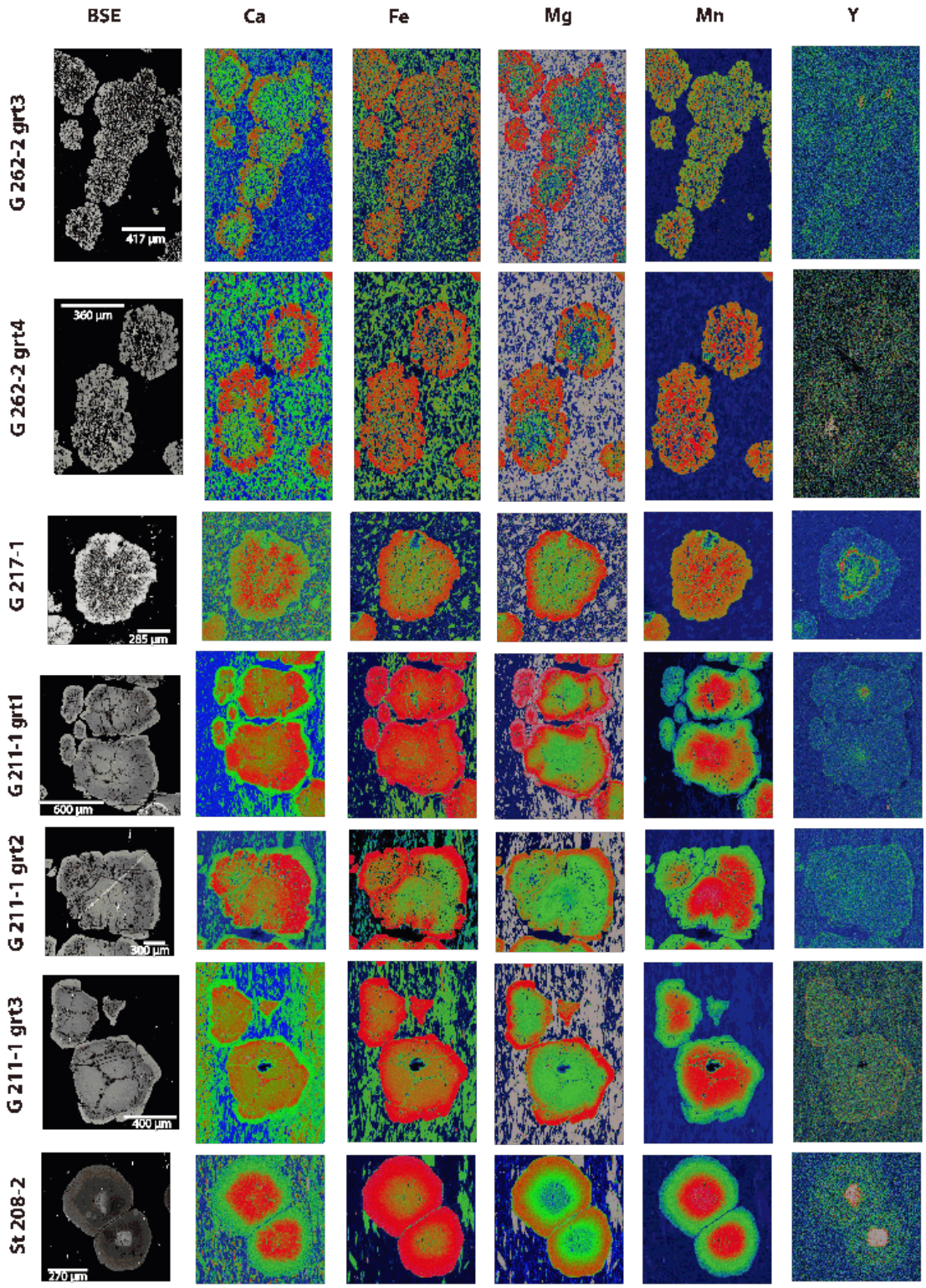

Figure 5 continued.

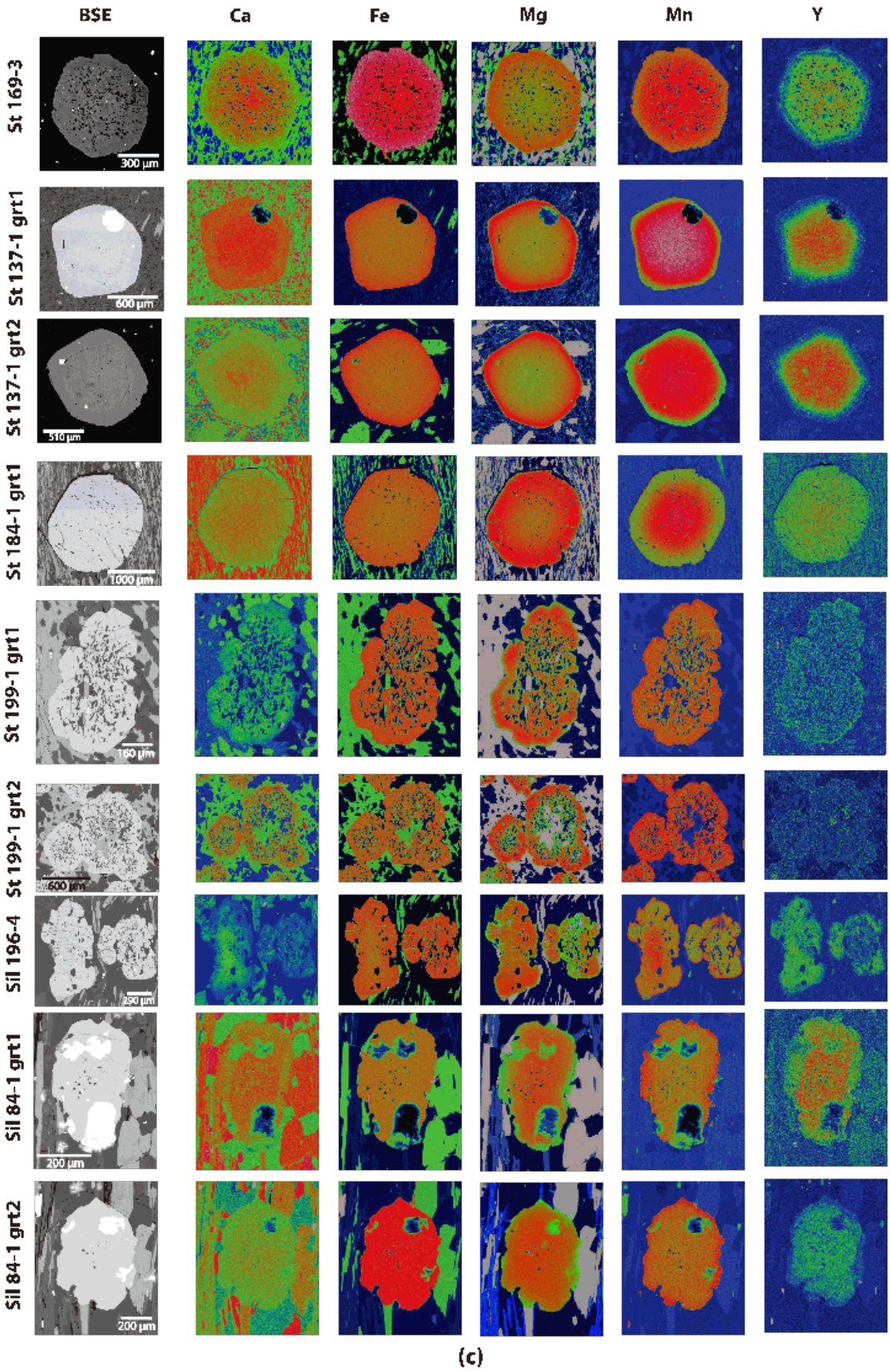

Figure 5 continued.

Staurolite zone

In the staurolite zone, garnet contains fewer inclusions. The BSE image for garnet in sample 208-2 contains a very bright core, dark mantle around the core and a relatively bright, inclusion-free rim (Figure 5). The very bright core corresponds to high-Y concentrations, whereas the outer edge of the mantle corresponds precisely to onset of low Ca concentrations. Zoning of Fe, Mn, Mg and Y is similar to sample 211-1 in the garnet zone. The two samples are close to each other near the Thompson Draw synform (Figure 1). However, Ca zoning in the samples is different. The high Ca core in 208-2 also corresponds to elevated Mn and relatively low Fe and Mg concentrations. The zoning of these elements is more diffuse than that of Ca. Garnets in samples 169-3, 137-1 and 184-1 have large, rather homogeneous cores with elevated Ca, Mn, and Y, whereas Fe, Mg are relatively depleted. Ca and Y define well interior dodecahedral garnet shapes (Figure 5). Sample 199-1, which is near the axis of the Thompson Draw synform, is nearly homogeneous except for patchy Y zoning in grt1. Garnets within this sample are morphologically similar to low grade garnets. For all other samples in the staurolite zone, Mn concentrations are high in garnet cores, but they do not correspond to the dark or bright regions of BSE images. Fe and Mg concentrations rise from core to rim and their zoning also does not correspond to the brightness of BSE zones. Large biotite inclusions in garnet within sample 199-1 suggested that it was not fully recrystallized.

Sillimanite Zone

In the sillimanite zone, which is largely within the strain aureole of the HPG, garnets have few inclusions. Zoning is more limited than in the lower-grade zones. In

garnets of sample 84-1, Ca concentrations are fairly uniform and relatively high throughout, except in rims. Y is also high in the cores. Fe zoning is not obvious. Mn is generally uniform, but it displays a high annulus at rims. Mg concentrations are fairly uniform except at rims where they are lower. Garnets in 196-4 shows more patchy zoning, and Fe and Mg concentrations increase from core to rim, whereas Mn has a higher concentration in the core. The morphology and zoning in garnets of this sample suggests that the garnets partially preserve a lower-grade P-T history.

Zoning of Ti

Some garnets in the garnet and staurolite zones show zoning of Ti with higher concentrations in cores than rims (Figures 6). Low Ti in rims may indicate an increasing competition for Ti by biotite. In the staurolite and sillimanite zones, Ti appears to be patchy with elevated Ti probably marking locations of ilmenite and biotite.

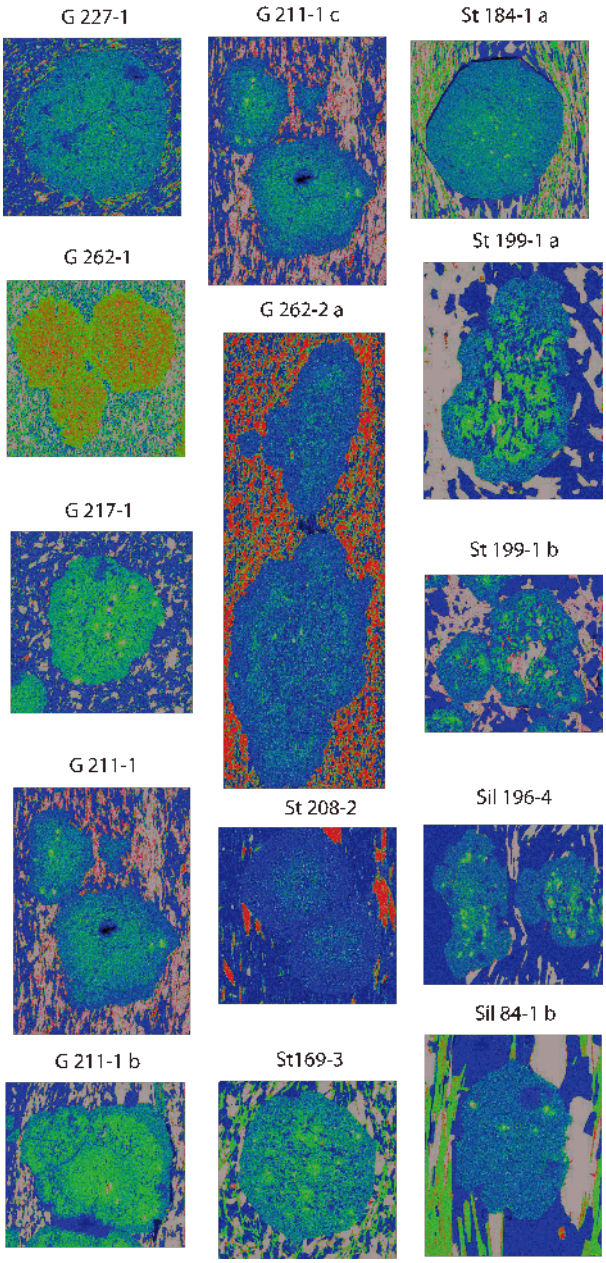

Figure 6 Ti zoning in some samples in the Black Hills.

Summary of X-ray maps

For major elements, Ca concentrations are relatively low in garnet cores in the garnet zone but are relatively high in garnet cores in both the staurolite and the sillimanite zones. Fe concentrations are higher in rims in all three metamorphic zones if garnets

display zoning. All garnets in the garnet and staurolite zones have low-Mg cores, but Mg concentrations are higher in cores in the sillimanite zone. Mn displays higher concentrations in cores in the garnet and staurolite zones but lower concentrations in cores in the sillimanite zone within the high-strain aureole. The zoning of Fe, Mn and Mg is more diffuse than the zoning of Ca, Ti and Y. Y concentrations are mostly higher in garnet cores in all metamorphic zones. In particular, high Ca, Ti and Y concentrations are prevalent in well-defined dodecahedral regions of garnets, both in garnet interiors and in rims. Broad high-Ca and Y cores are particular prevalent in the region between the Hill City and Keystone faults.

Compositional profiles

Compositional profiles across selected garnets produced by EPMA were normalized to 12 oxygens (Appendix I) and the four major components, almandine ($Fe_3Al_2Si_3O_{12}$), spessertine ($Mn_3Al_2Si_3O_{12}$), pyrope ($Mg_3Al_2Si_3O_{12}$) and grossular ($Ca_3Al_2Si_3O_{12}$) were calculated (Appendix II). The compositional profiles are shown in Figure 7a-i.

Garnet zone

All garnets in the garnet zone have similar profiles and are in agreement with the element maps. X_{grs} increases systematically from cores toward rims but then decreases in inclusion-poor overgrowths. X_{grs} in cores is 0.08 to 0.1. X_{alm} ranges from 0.45 to 0.5 in the cores. In all garnets, X_{alm} then increases substantially in the overgrowths while X_{sps} has opposite profiles. In cores it ranges from 0.43 to 0.35, with progressively lower values toward higher grades. The exception is the lowest-grade garnet in 227-1 in which Fe is fairly invariable but X_{sps} decreases from 0.46 in the core and then varies inversely with X_{grs} (Figure 7a). All garnets have invariable Mg in cores, but it is slightly more elevated in overgrowths, except in 227-1 where Mg is effectively invariable.

Staurolite zone

A garnet in sample 208-2 (Figure 7e) has a high-Ca core with X_{grs} at ~ 0.1 that is similar to cores in the garnet zone. X_{grs} decreases to ~0.02 in the rim. In sample 137-1,

X_{grs} decreases from ~0.05 in core to 0.03 in the rim. Low-Fe and high-Mn garnet core region in sample 208-2 is apparently narrower than core regions of other garnets, but that may be because the garnet was cut a distance from the center. X_{alm} increases from 0.52-0.70 in cores to 0.80-0.82 in the rims. Mn is zoned inversely from Fe. In all samples, X_{py} is ~0.04 in the cores, increase towards ~0.1 in overgrowths, and then decreases to ~ 0.08 at the very rims. Garnet in sample 199-1 is effectively unzoned with X_{sps} = 0.23 and X_{alm} = 0.65.

Sillimanite zone

Garnet in the representative sample 84-1 displays relatively flat composition profiles. X_{grs} is ~0.4 and X_{alm} is ~ 0.78. X_{sps} is 0.11 in the core but slightly increases to 0.15 at the rim. X_{py} decreases from 0.09 in the core to 0.05 in the rim.

Summary of composition profiles

Almandine concentrations are the highest of all the four garnet end-members. X_{sps} varies inversely from X_{alm}. From the garnet zone to the staurolite zone, X_{alm} increases from cores to rims. The zoning of almandine and spessartine is most intense in the upper garnet and the staurolite zones (Figure 7a-f). As noted previously (Nabelek et al. 2006), spessartine-rich garnets are more abundant in the lower garnet zone but unzoned, almandine-rich garnets are dominant in the sillimanite zone.

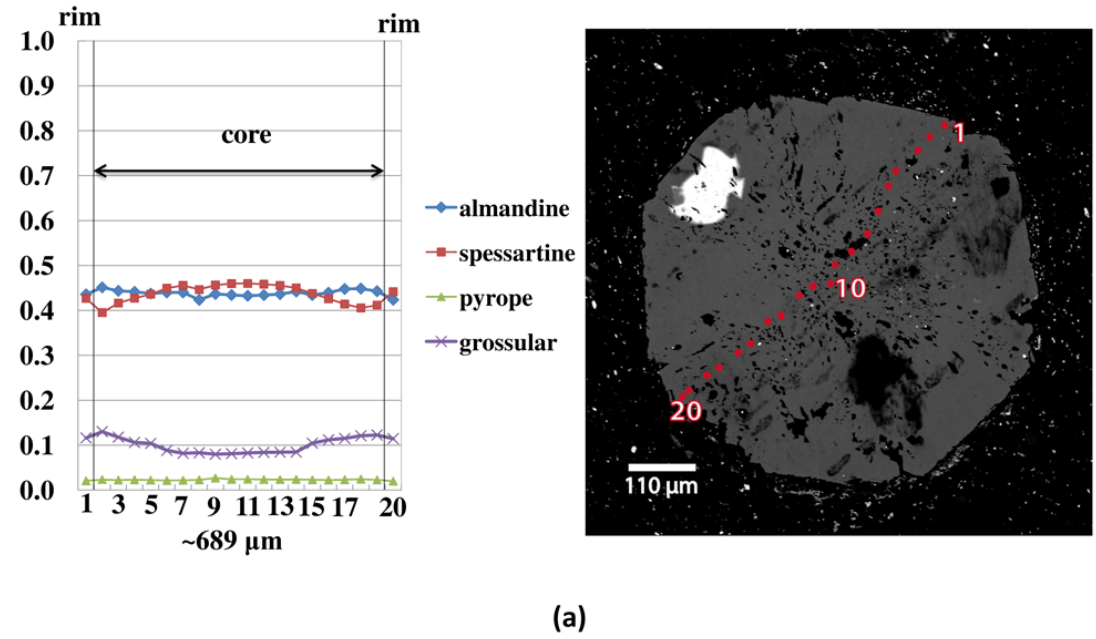

Figure 7 Rim to rim chemical compositional variations for garnets from the garnet, staurolite and sillimanite zones. The numbers under the diagram are the approximate lengths of the traverse on the photos. X_{alm} and X_{sps} are similar at low grades. With closer distance to the HPG intrusions, X_{alm} increase and X_{sps} decrease from core to rim. X_{alm} and X_{sps} are homogeneous at high grades. X_{grs} is lower than the proportion of almandine and spessartine. X_{py} is the lowest and has relatively flat variation profiles.

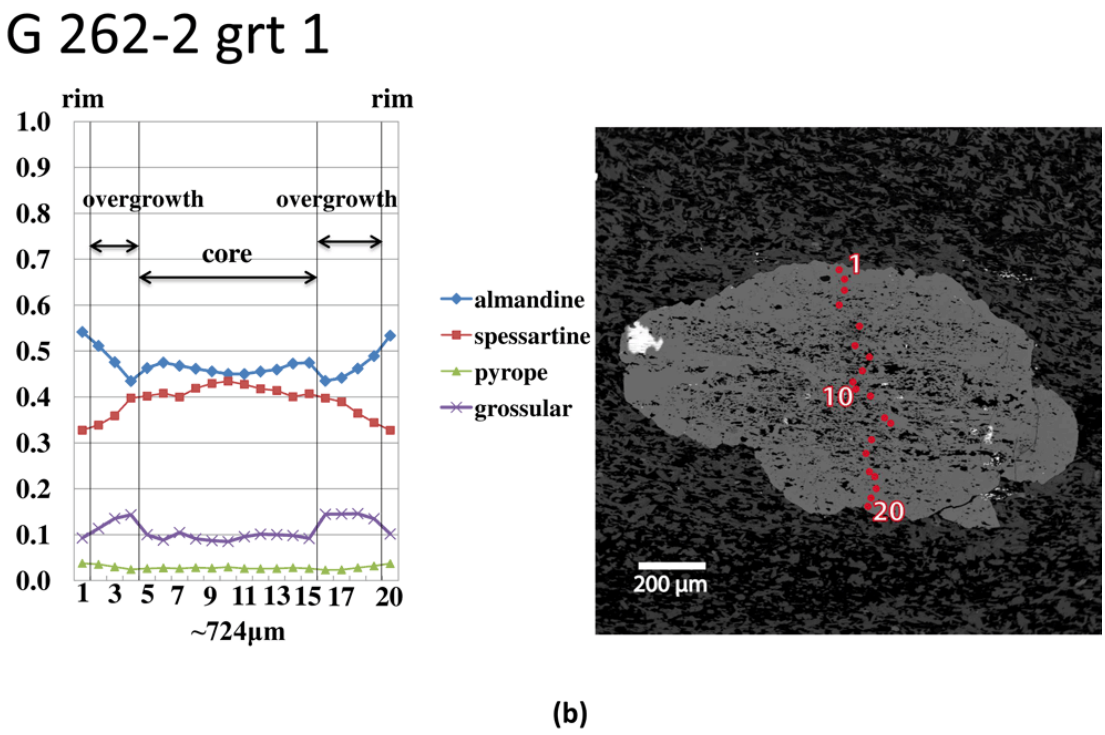

(b)

Figure 7 continued.

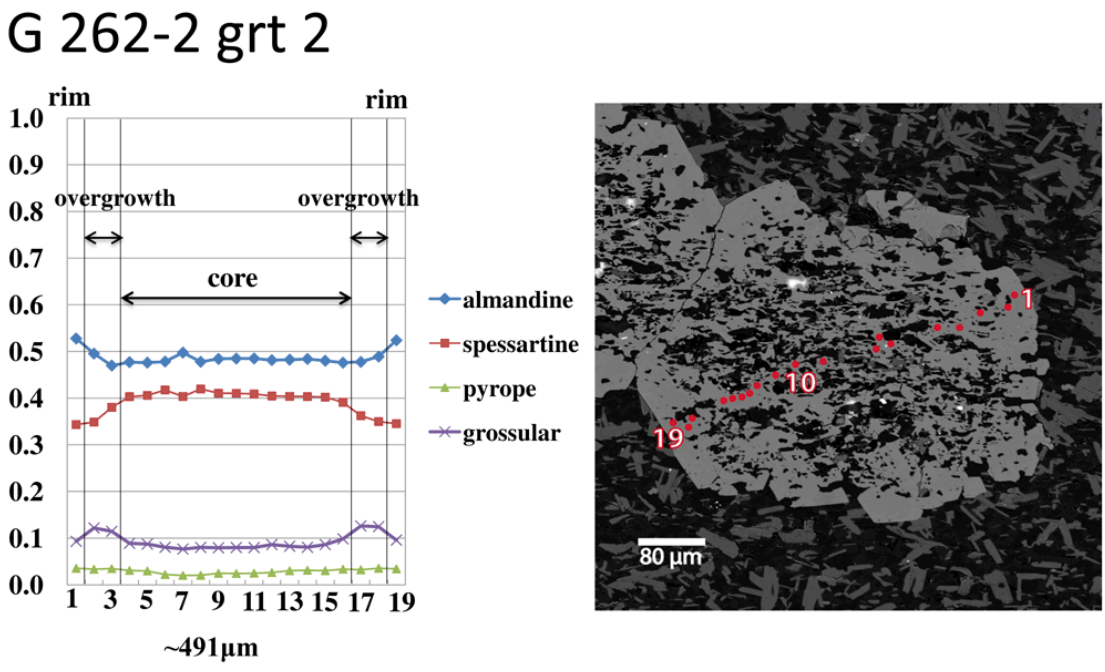

(c)

Figure 7 continued.

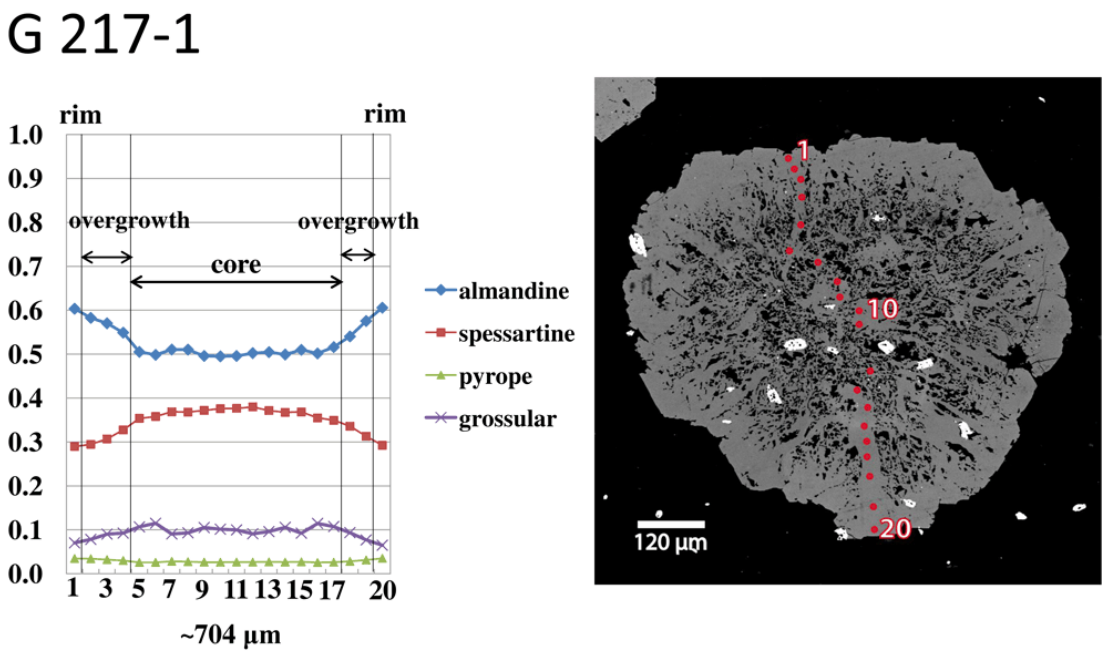

(d)

Figure 7 continued.

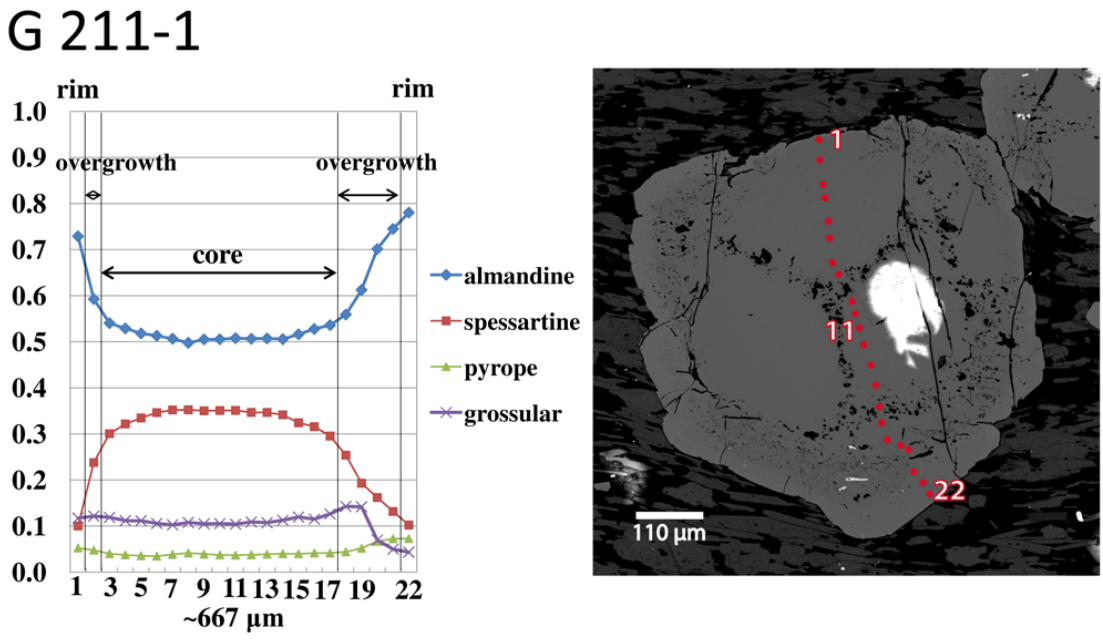

(e)

Figure 7 continued.

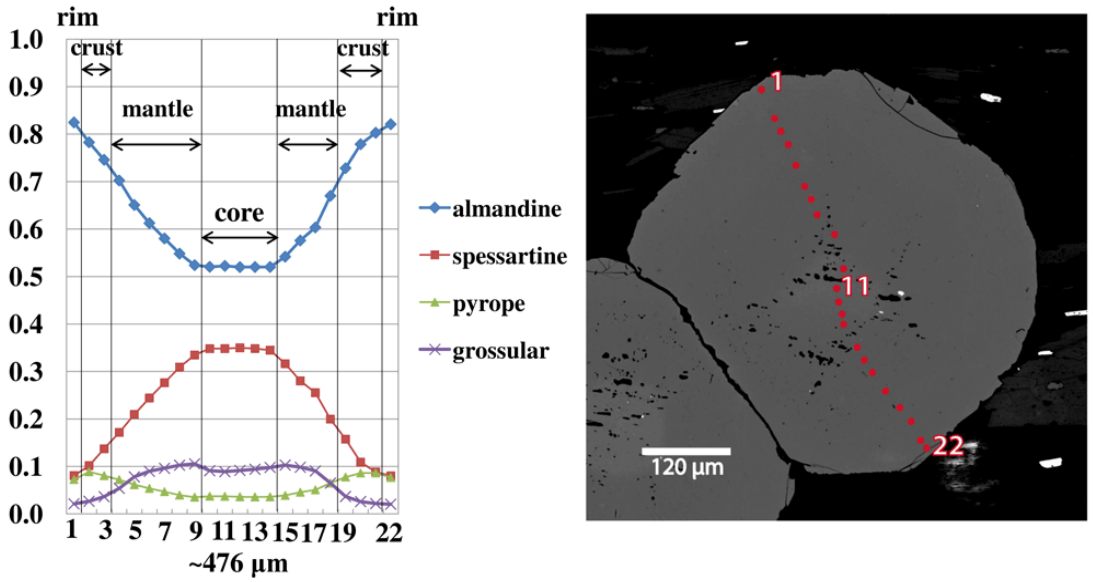

Figure 7 continued.

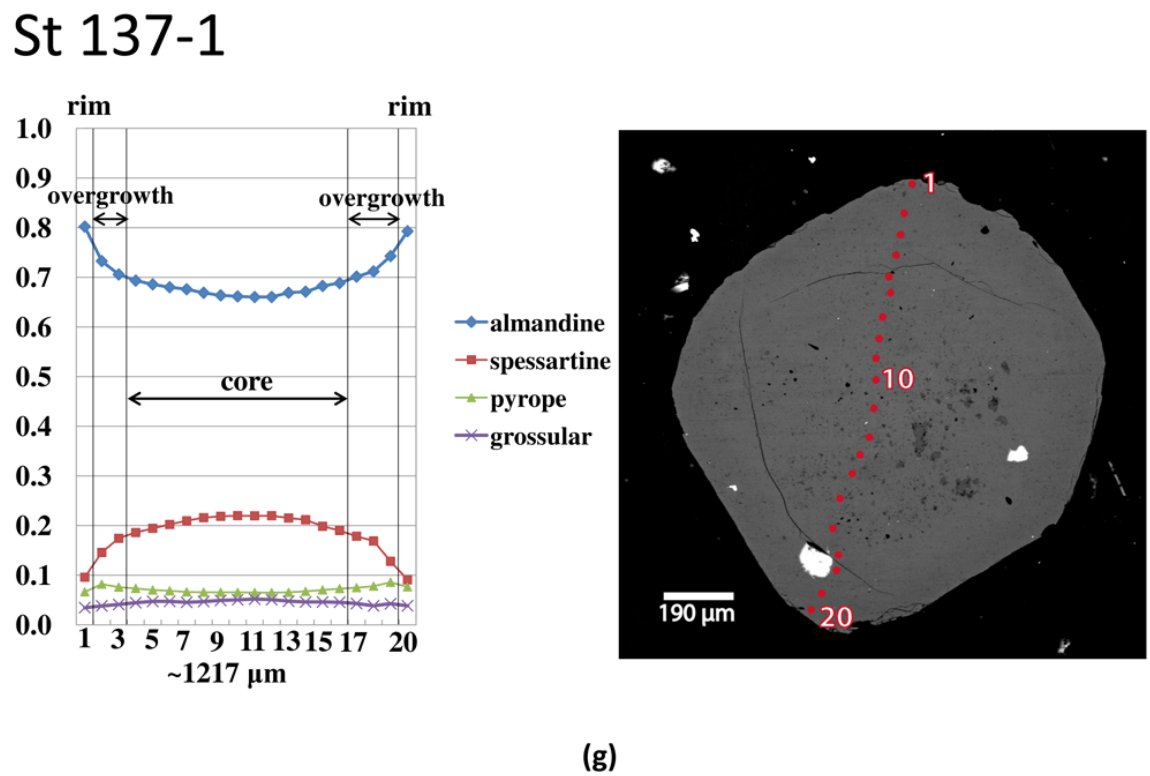

Figure 7 continued

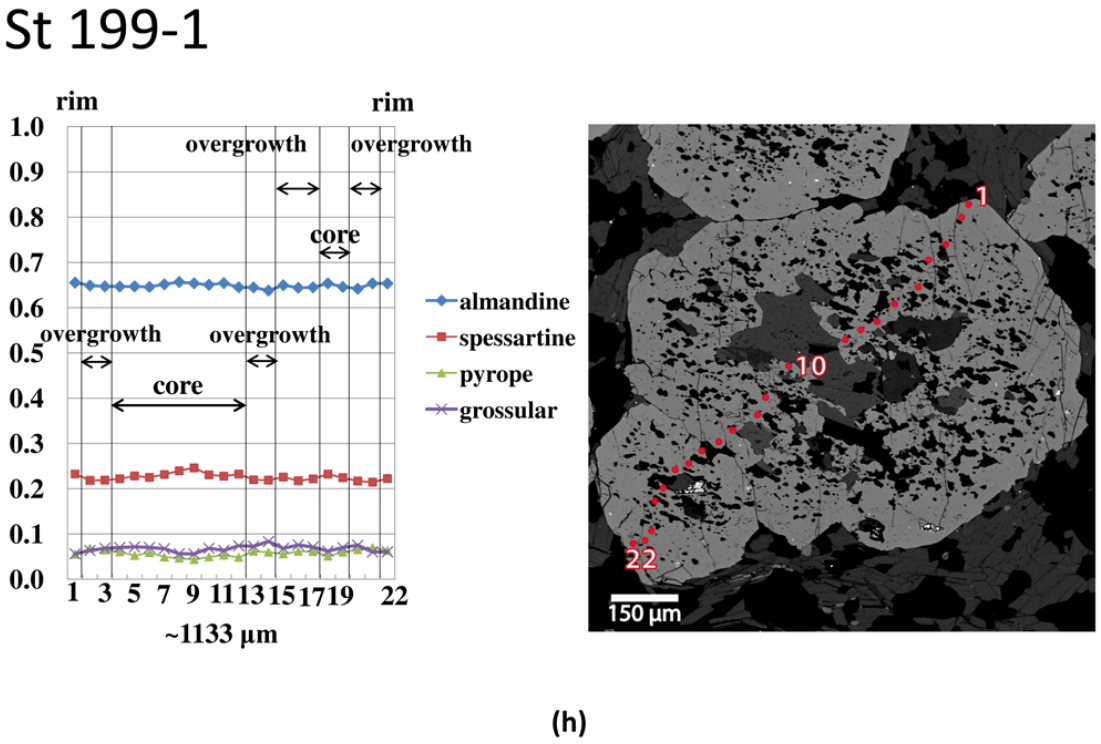

(h)

Figure 7 continued.

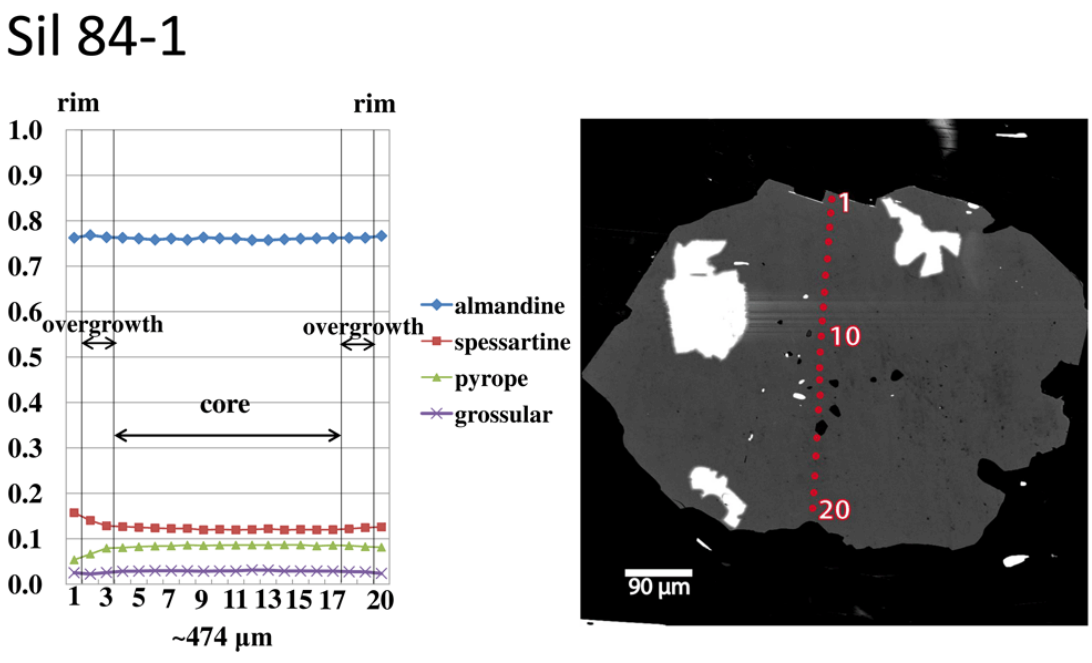

(i)

Figure 7 continued.

Pseudosections

Table 1 Average composition of metapelites in the Black Hills (Nabelek et al. 2006) and the average composition with higher Al_2O_3.

	Average metapelite	**Metapelite + 2.5% Al_2O_3**
SiO_2	62.3	60.5
TiO_2	0.68	0.66
Al_2O_3	17.1	19.5
FeO	7.44	7.22
MnO	0.34	0.33
MgO	2.54	2.46
CaO	0.52	0.50
Na_2O	1.43	1.39
K_2O	4.42	4.29
P_2O_5	0.13	0.13
H_2O	1.69	1.64

Equilibrium phase-assemblage diagrams (pseudosections) with garnet composition contours, for almandine, spessartine, grossular and pyrope, were constructed with the program THERIAK-DOMINO (Capitani and Petrakakis, 2010) using the thermodynamic database "tcdb55" (updated from Holland and Powell, 1998). First pseudosection was constructed for the average composition of ~30 Black Hills metapelites (Table 1; Nabelek et al., 2006). The pseudosection shows assemblages that occur in the Black Hills, including garnet + chlorite, garnet, garnet + staurolite, garnet +

sillimanite, garnet + andalusite, and garnet + cordierite, in addition to plagioclase, muscovite (or K-feldspar), biotite and quartz in each field (Figure 8a). However, the pseudosection shows only a very narrow staurolite-present field that is inconsistent with the rather broad distribution of staurolite in the aureole of the HPG, and a broad cordierite field that is inconsistent with the only occasional occurrence of cordierite in the field. With addition of 2.42 wt. % Al_2O_3 (Table 1), the staurolite field becomes considerably larger (Figure 8b) and more consistent with field observations.

A pseudosection with 19.5 wt.% Al_2O_3 was also constructed for $a(H_2O) = 0.8$ to reflect reduced activity of H_2O that is evident in fluid inclusions in quartz veins (Huff and Nabelek, 2007). For $a(H_2O) = 1$ (Figure 8b), the biotite + garnet field is smaller than field observation, possibly because the actual low H_2O activity caused the reaction of chlorite to garnet at a lower temperature (Nabelek et al. 2006). For $a(H_2O) = 0.8$ (Figure 8c), assemblage boundaries move to lower temperatures. The muscovite dehydration reaction occurs within the sillimanite field below the solidus, which it is not consistent with the petrographic observations that muscovite breakdown lead to partial melting. Therefore, the pseudosection with 19.5 wt.% Al_2O_3 and $a(H_2O) = 1$ was used in this study.

For all the pseudosections, equilibrium garnet growth was assumed. The pseudosections do not reflect possible effective change in rock composition due to fractional growth of garnet (Spear, 1993; Vance and Mahar, 1998). In the equilibrium growth model, small variations of bulk composition do not influence greatly garnet composition contours. For the exchange of Fe and Mg between garnet and biotite, for example, even though the relative amounts of minerals may change with variation in bulk composition and $a(H_2O)$, the equilibrium constant for Fe and Mg does not change at a

given pressure and temperature. Thus, the applied pseudosection reasonably reflects pressure and temperature changes of aluminous Black Hills metapelites.

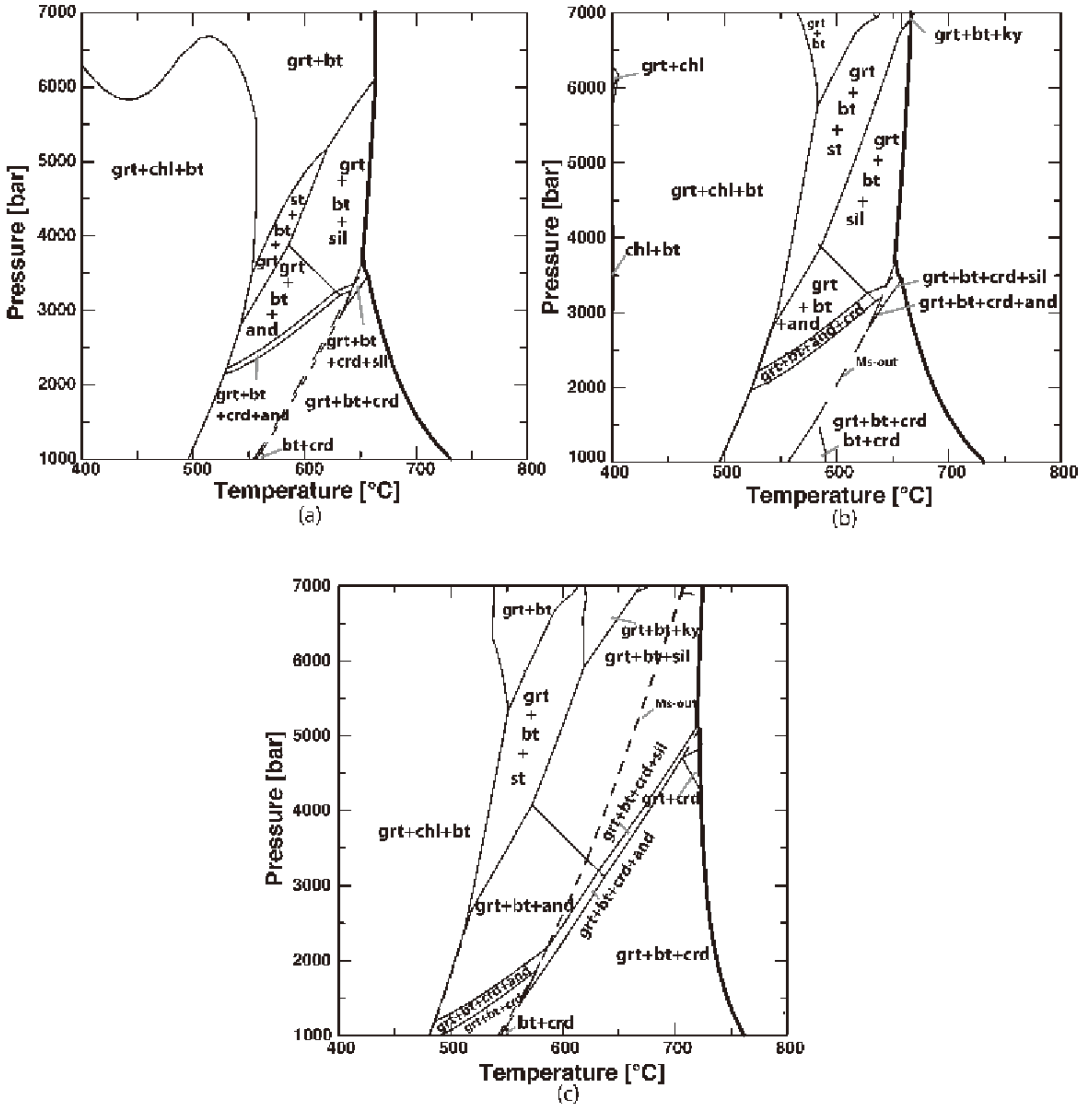

Figure 8 Pseudosections calculated by THERIAK-DOMINO (Capitani and Petrakakis, 2010). (a) Pressure and temperature equilibrium diagram produced by using average metapelite compositions in table 1 (Nabelek et al. 2006). (b) Pressure and temperature equilibrium diagram calculated with higher-Al metapelite compositions in table 1 and using $a(H_2O)=1$. (c) Pressure and temperature equilibrium diagram calculated using same data as (b), but with $a(H_2O)=0.8$.

Predicted garnet composition contours are shown in Figure 9. X_{alm} and X_{pyr} increase with temperature in the garnet + biotite + chlorite field while X_{sps} decreases

(Figure 9a, b, d). In the staurolite and sillimanite-present fields, these components are more pressure-dependent. Contours of X_{grs} depend on both temperature and pressure throughout the illustrated P-T regime (Figure 9c).

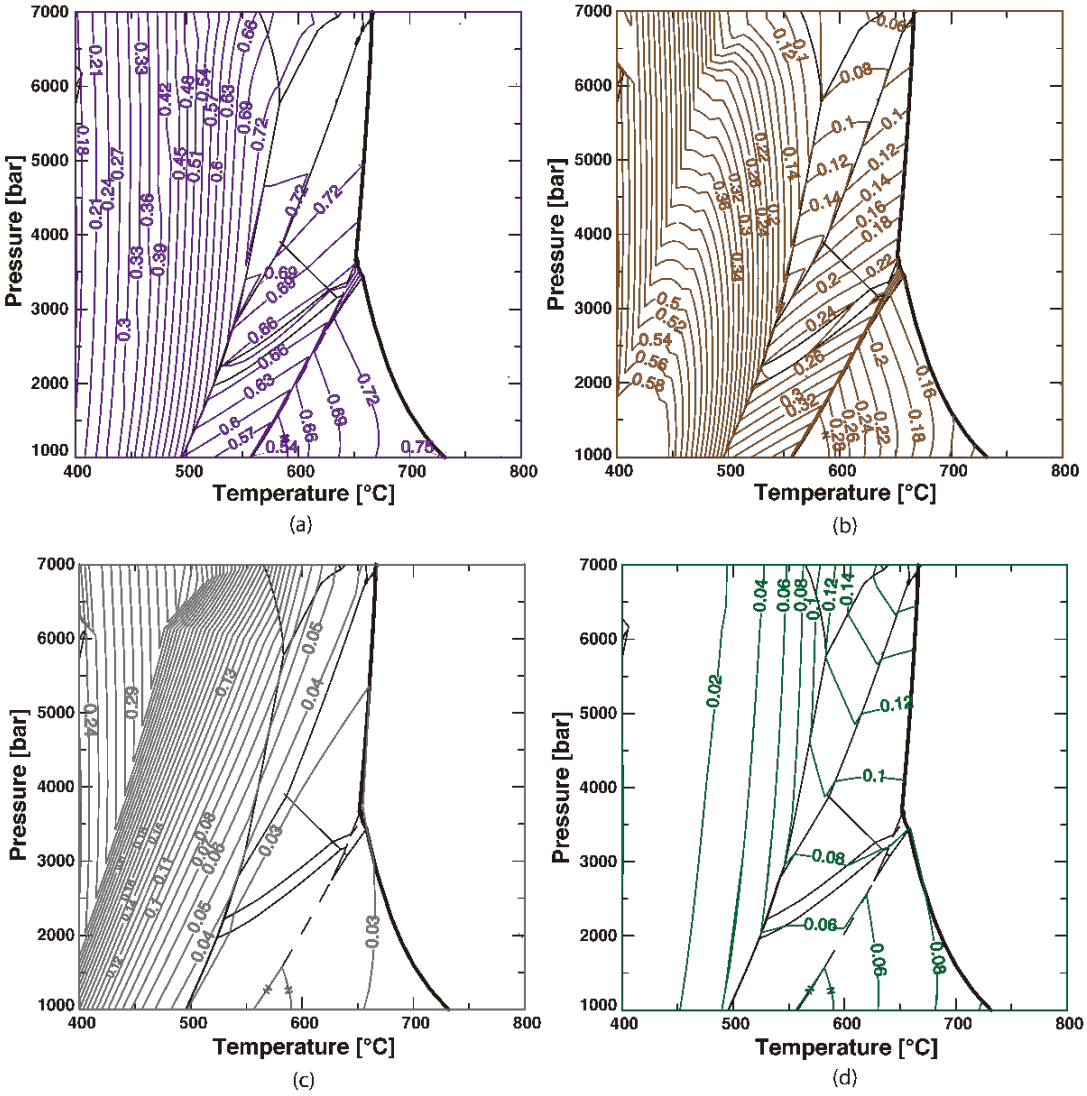

Figure 9 Contours of garnet end-members calculated by THERIAK-DOMINO. (a) Almandine (b) Spessartine (c) Grossular (d) Pyrope

P-T-t paths during garnet growth

The garnet compositions (Appendix II) were used to determine apparent P-T-t paths of the host rocks during garnet growth by superimposing fractions of their components on the contoured pseudosection (Figure 9). As X_{py} is very low in all garnets, pyrope was not used in determining P-T-t paths. Combinations of almandine-spessartine, almandine-grossular and spessartine-grossular show consistent results.

Garnet zone

The P-T-t paths for samples in the garnet zone indicate pressure changes during garnet growth. Sample 227-1 has a low-pressure core with compositions giving 2400 to 2800 bar (Figure 10a). Apparent pressure increased gradually from core to rim until it reached the maximum value of ~3900 bar. The very rim indicates pressure of ~3000 bar. A slight increase in temperature, from 485^{o}C to 490^{o}C is indicated. For sample 262-2, core compositions indicate pressure of ~2800 bar to ~3600 bar with subsequent increase to ~4400 bar toward rims. The very rims again show a slight decrease in pressure (Figure 10b, c). Temperature of these two garnets slightly increased from 480^{o}C during growth of cores to 510^{o}C during growth of overgrowths. For sample 217-1 (Figure 10d), the indicated pressure ranges from ~3100 bar in garnet core up to ~4000 bar in overgrowths and then decreases to ~3000 bar at the very rim. The indicated temperature ranges from 490^{o}C to 510^{o}C. It is thus evident that these samples may have undergone a nearly isothermal pressure increase during the growth of the garnets with a possible reduction in pressure during growth of narrow rims. The initial pressure at which garnet grew appears to have been lower in the lower garnet zone that is represented by sample 227-1.

The highest pressure in the garnet zone is indicated by garnet within sample 211-1, which is near the staurolite isograd. In this sample, apparent pressure increased from 3600 bar during growth of cores to nearly 6000 bar during growth of inclusion-free rim. There is a jump in temperature from ~500°C for the core to 600°C for the rim. The indicated pressures and temperatures by the rim composition are somewhat scattered, but it is notable that they fall within the staurolite field (Figure 10e).

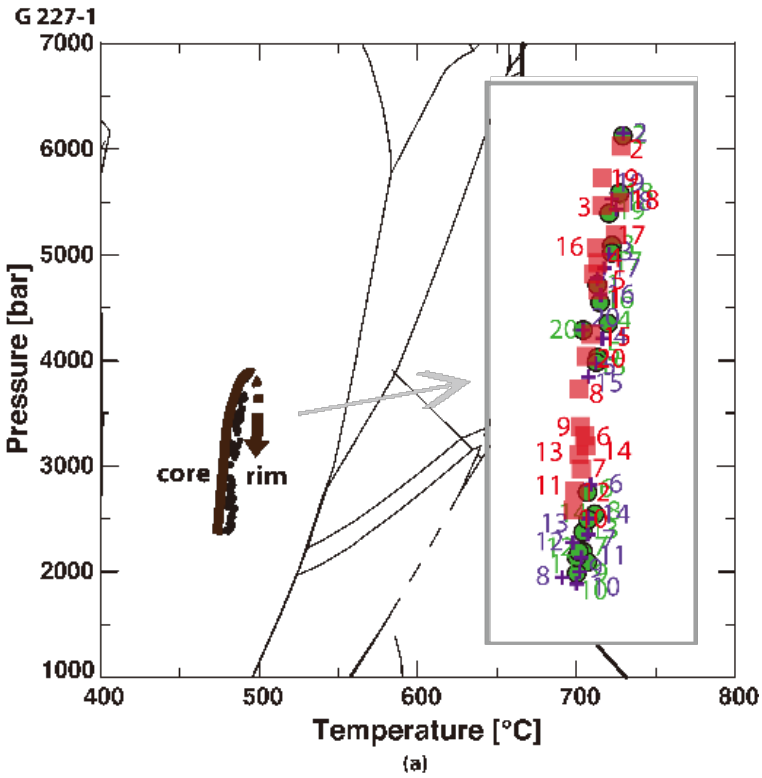

Figure 10 Pressure and temperature paths during garnet growth determined from chemical compositions and contours in Figure 9. Red squares are from combination of almandine and spessartine contours; Purple crosses are from combination of almandine and grossular contours; Green circles are from combinations of spessartine and grossular contours. Numbers aside the circles correspond to points in the compositional profiles (Figure 7). Solid symbols represent accurate intersections of the contours. Empty symbols are approximate positions, because some of the compositions measured by EPMA are higher than the contours calculated by THERIAK-DOMINO. The empty symbols were plotted using the intersections of the highest values of the contours.

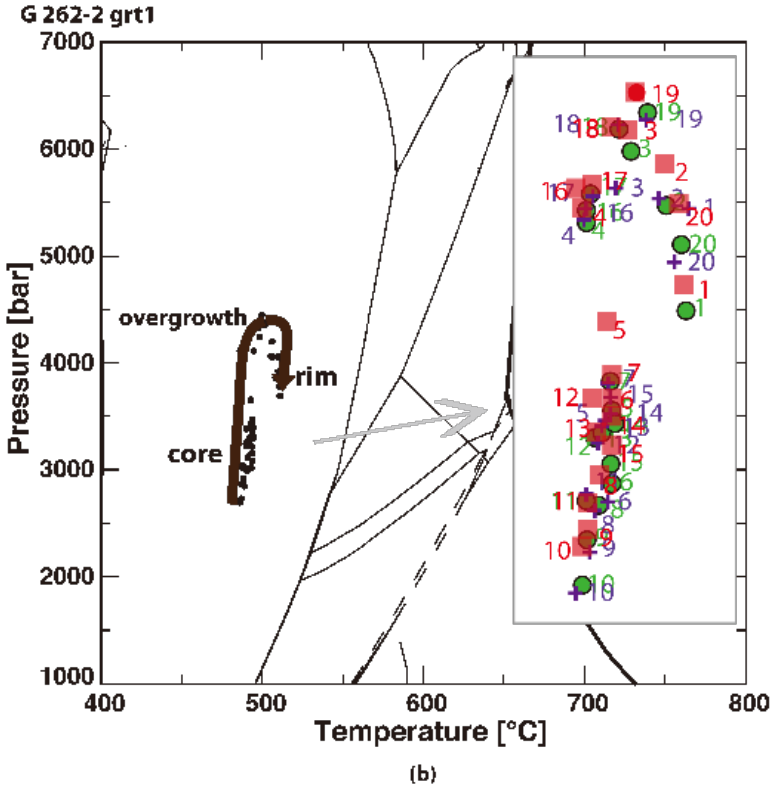

Figure 10 continued.

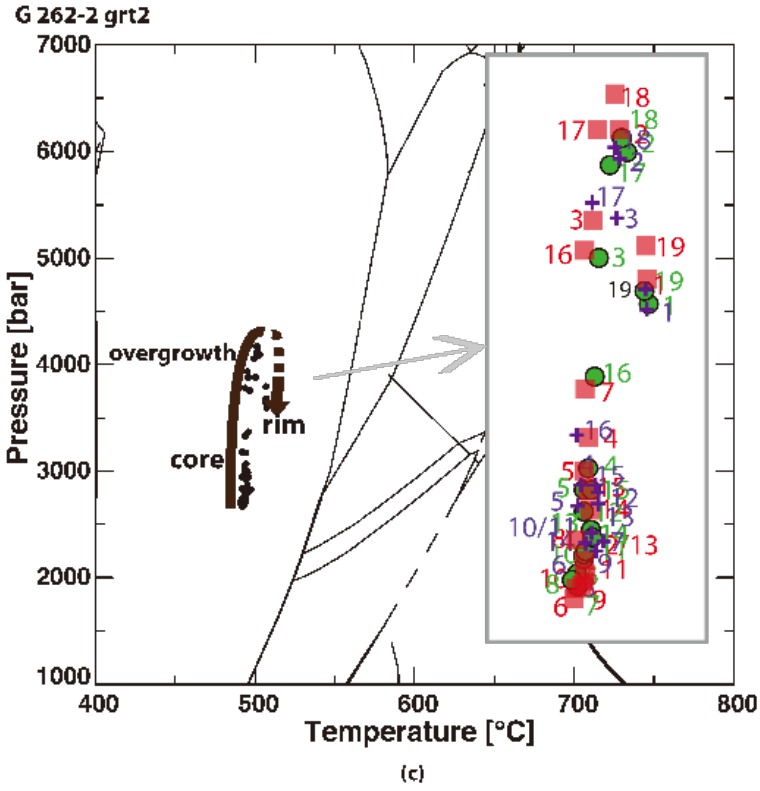

Figure 10 continued.

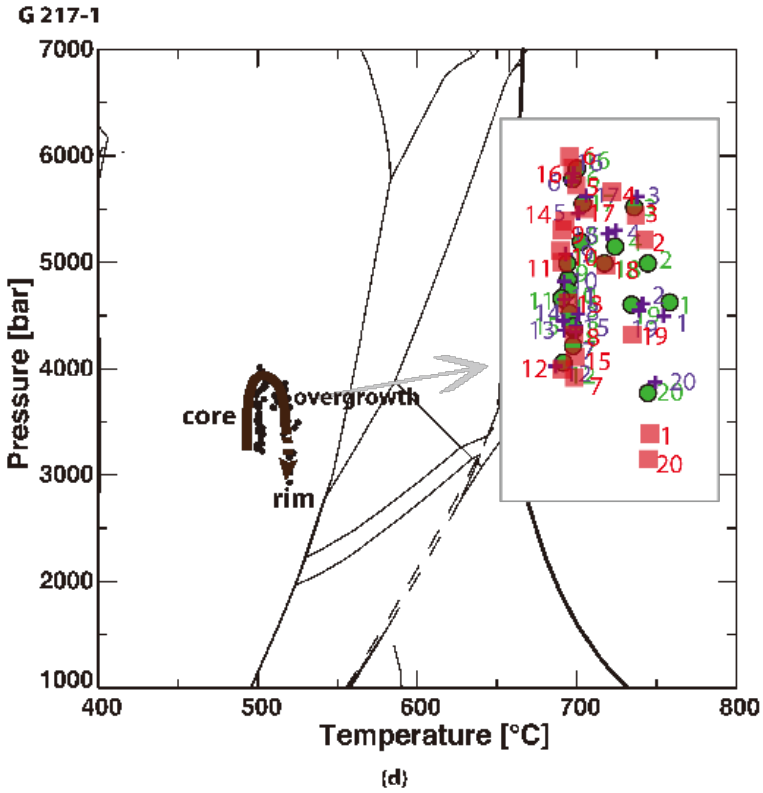

Figure 10 continued.

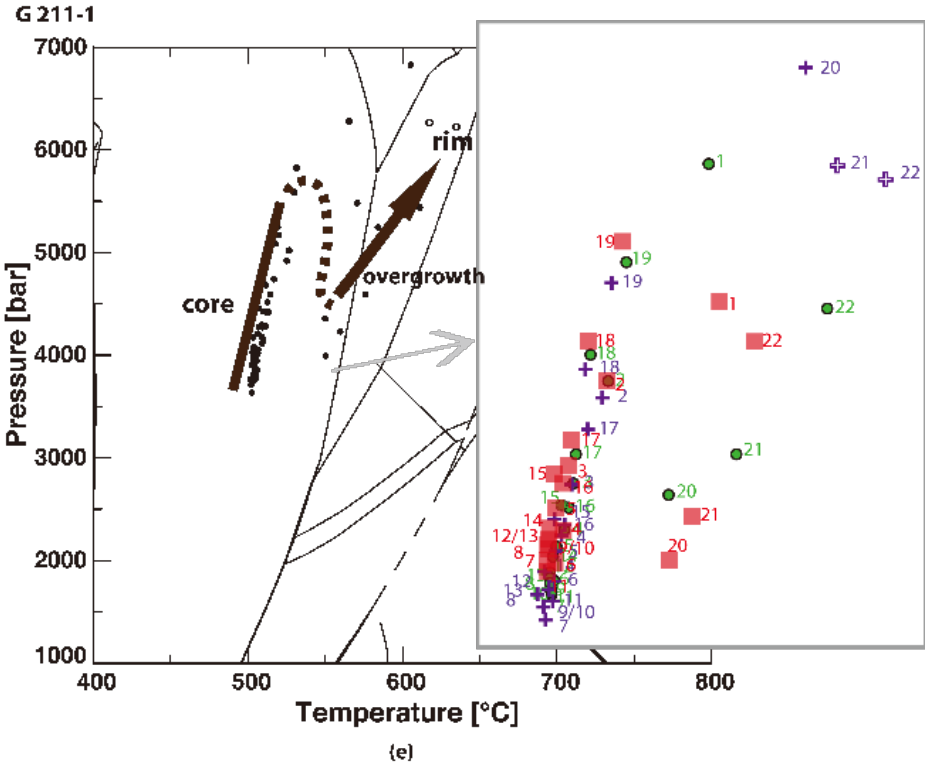

Figure 10 continued.

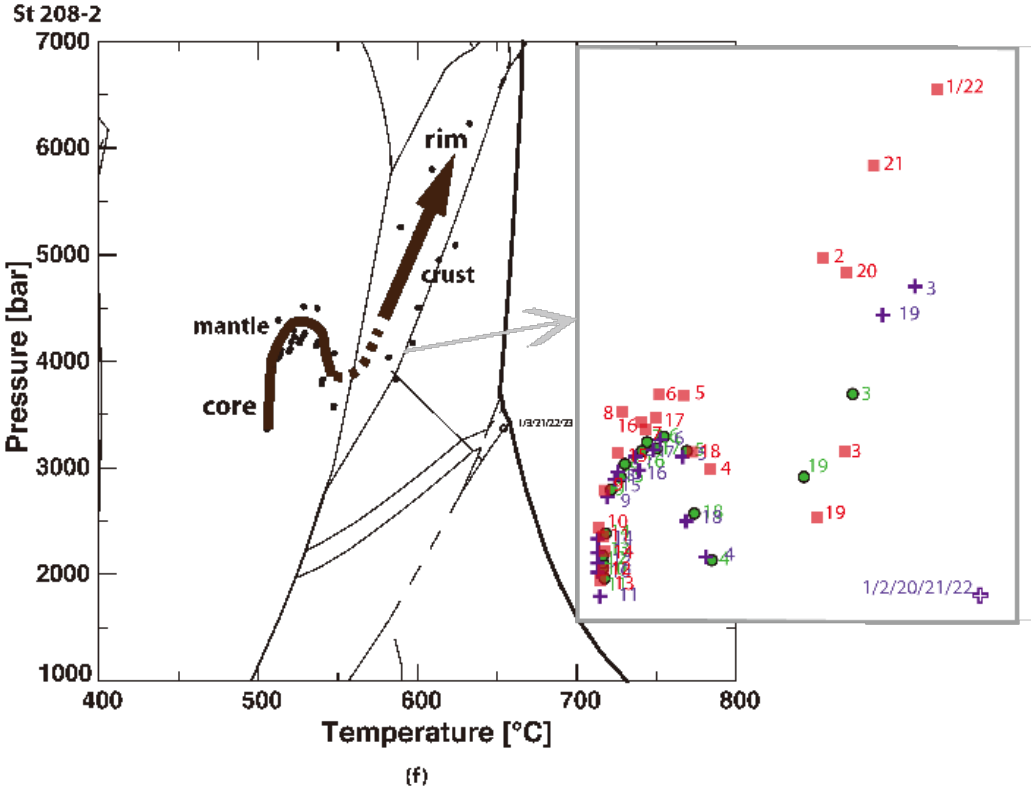

Figure 10 continued.

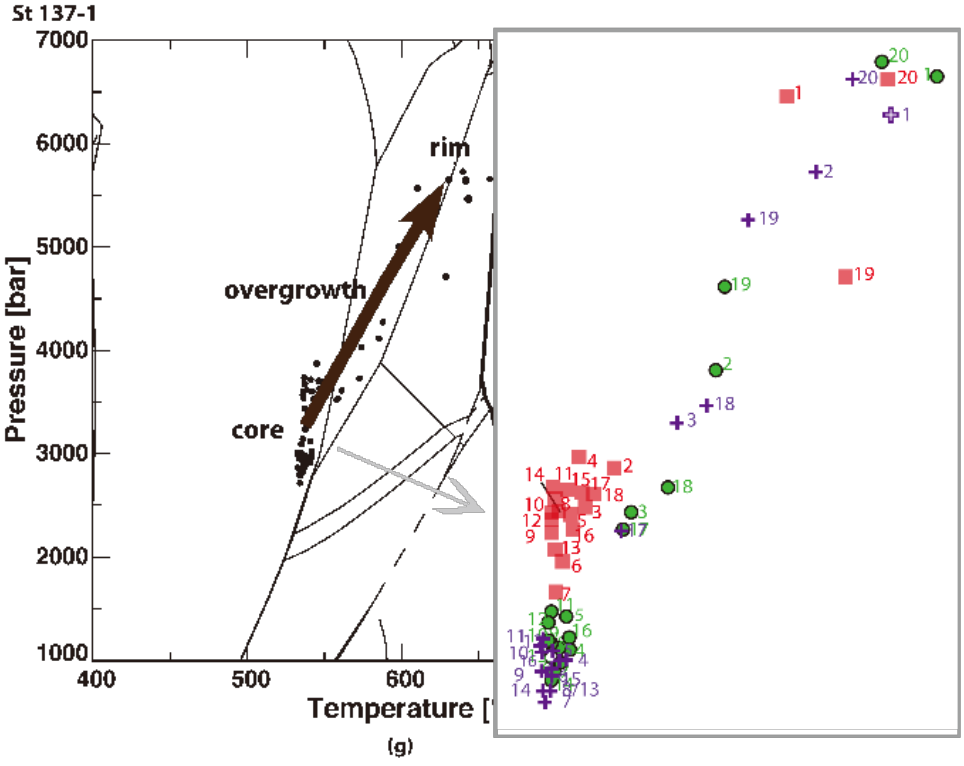

Figure 10 continued.

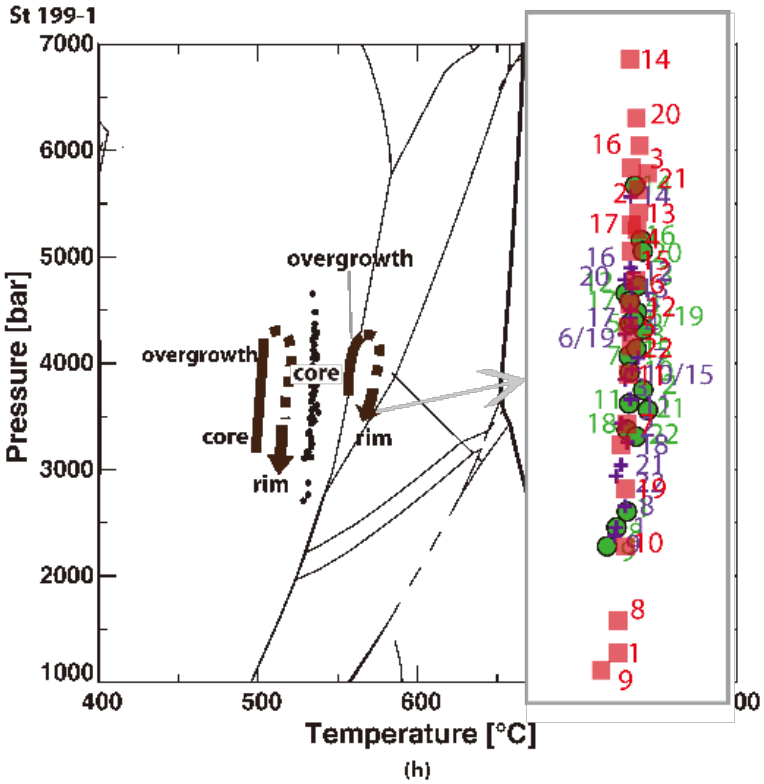

Figure 10 continued.

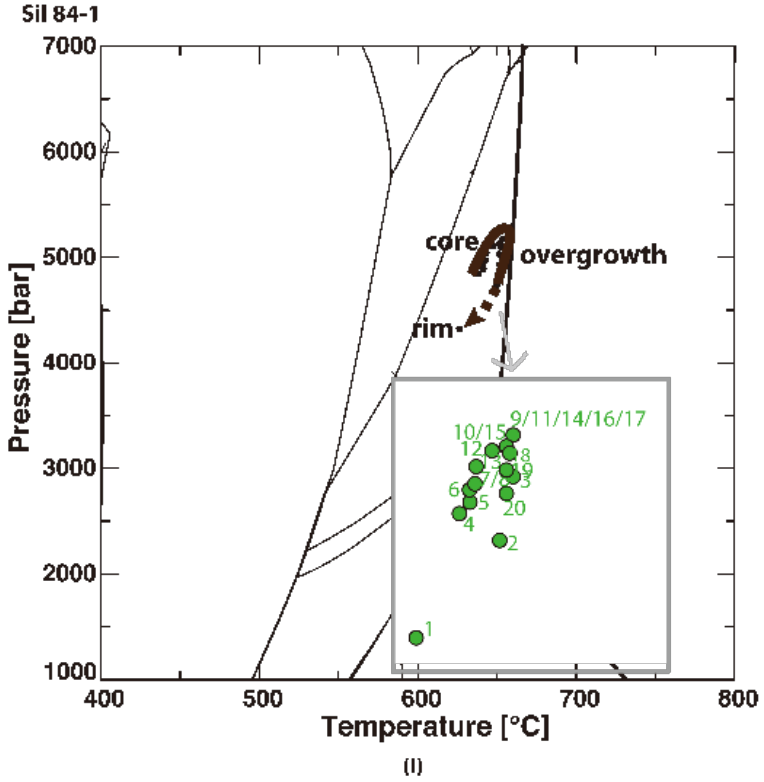

Figure 10 continued.

Staurolite zone

For sample 208-2, indicated pressure is ~3400 bar for the bright core in the BSE image and increases towards the rim to ~4400 bar (Figure 10f). Indicated temperature increases from 500^{o}C to 540^{o}C. For sample 137-1, apparent pressure increases from core at ~3000 bar to rim at ~5500 bar and temperature increases from core at ~535^{o}C to rim at ~600^{o}C (Figure 10g). For sample 199-1, the P-T-t paths are shown for two garnets that occur near each other (Figure 10h). Indicated core-pressure of the larger garnet is ~ 3100 bar, increased to ~4300 bar towards the rim and decreased to ~2900 bar at the very rim. The small garnet has indicated pressure elevated from ~3600 bar to ~ 4300 bar and then declined to ~ 3500 bar at the rim. However, rims of the two garnets where they are in contact with each other do not have obvious low-pressure rims. Temperature is nearly constant at ~540^{o}C.

Sillimanite zone

For sample 84-1, it is only possible to plot garnet compositions using intersections of spessartine and grossular contours (Figure 10i). The other sets of contours do not intersect in the P-T range of the diagram. Apparent pressure decreased from the core at ~5000 bar towards the rim at ~4250 bar. It grew in a fairly uniform temperature at ~650^{o}C except for the very rim.

Summary of P-T paths

The garnets show apparent temperature increases by more elevated Fe and Mg concentrations and decreased Mn concentrations in rims. The pressure variations are primarily shown by Ca zoning. They suggest nearly isothermal pressure increase for low-grade rocks and more elevated pressures during growth of inclusion-free sillimanite zone garnets.

Discussion

The purpose of this thesis is to address 1) the conditions of garnet growth in the Black Hills schists and 2) P-T-t paths of the different areas of the Black Hills. However, before these issues can be addressed, the possibility that zoning in garnets reflects diffusive modification of garnet chemistry during reheating associated with intrusion of the Harney Peak Granite has to be evaluated.

Equilibration by internal diffusion

Self-diffusion of elements within garnet depends on temperature (T), pressure (P) and oxygen fugacity (f_{O_2}). Diffusion rates are related to garnet composition. The primary compositional influence is the unit-cell dimension of the divalent diffusing cations (Carlson, 2006). In order to quantify the divalent cation's diffusivity in garnets, the diffusion coefficient of a cation is determined by equation:

$$\ln D_i^* = \ln D_{o.i}^* + k(a_o - a_{o.i}) + \frac{-(Q + P\Delta V^+)}{RT} + \frac{1}{6}\ln(\frac{f_{O_2}}{f_{O_2}^{gr}}) . \quad [1]$$

(Carlson, 2006). $D^*_{0.i}$ is the frequency factor for diffusion in an end-member of garnet, including almandine, spessartine, pyrope and grossular, Q is Arrhenius activation energy, ΔV^+ is an activation volume, $a_{0.i}$ is the unit-cell dimensions of an end-member garnet, a_0 is the unit-cell dimension of whole garnet and is given by $X_{alm}a_{0.alm}+X_{py}a_{0.py}+X_{sps}a_{0.sps}+X_{grs}a_{0.grs}$, where $X_{0.i}$ is the mole fraction of an end-member (Appendix II). f_{O_2} and $f_{O_2}^{gr}$ were obtained from the estimated oxygen fugacities in the different metamorphic zones in the Black Hills (Huff and Nabelek, 2007). k stands for the

sensitivity of the frequency factor to unit-cell dimension. k of Ca is the highest and k of Mg is the lowest, implying that compositional variations have less influence on smaller ions than on larger ones (Carlson, 2006). Input values of temperature and pressure were taken from the pseudosections (Figure 10). Peak temperatures experienced by each garnet were used in calculations.

For garnets in all samples, except for grt2 in sample 262-2, $\ln D^*_{Fe^{2+}}$ varies from approximately –23 to –25, $\ln D^*_{Mn^{2+}}$ varies from approximately –25 to –27, $\ln D^*_{Mg^{2+}}$ is approximately –23, and $\ln D^*_{Ca^{2+}}$ is approximately –31 (Figure 11). Thus, the diffusivity of Mg was the highest whereas that of Ca was the lowest. For grt2 in sample 262-2, the calculated diffusivities are lower.

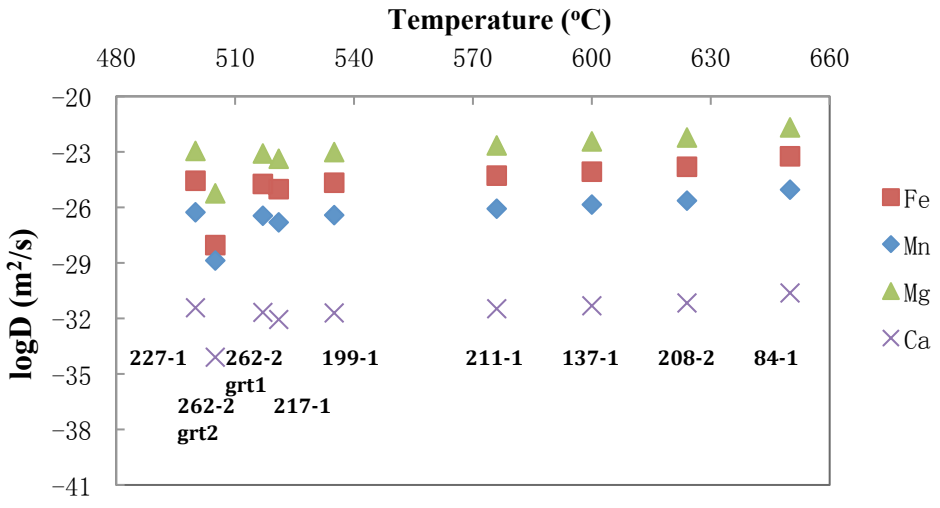

Figure 11 Diffusion coefficients for 2^+ cations in garnets from different metamorphic zones.

The characteristic diffusion distance for a diffusing species (Figure 12, Appendix III) is given by (Crank, 1975):

$$x = 2\sqrt{Dt}\ . \quad [2]$$

The conservative time of 45 Ma was used to calculate the diffusion distances, because it is the approximate interval between M_2 and M_3. As Mg diffuses faster than the other divalent cations, it has higher diffusion length scales. The model diffusion distances for Fe, Mn, and Ca are much smaller than their zoning scales in all the garnets. The distances of Mg are mostly higher than its observed zoning scales, but they are smaller than the radii of all garnets except in sample 84-1.

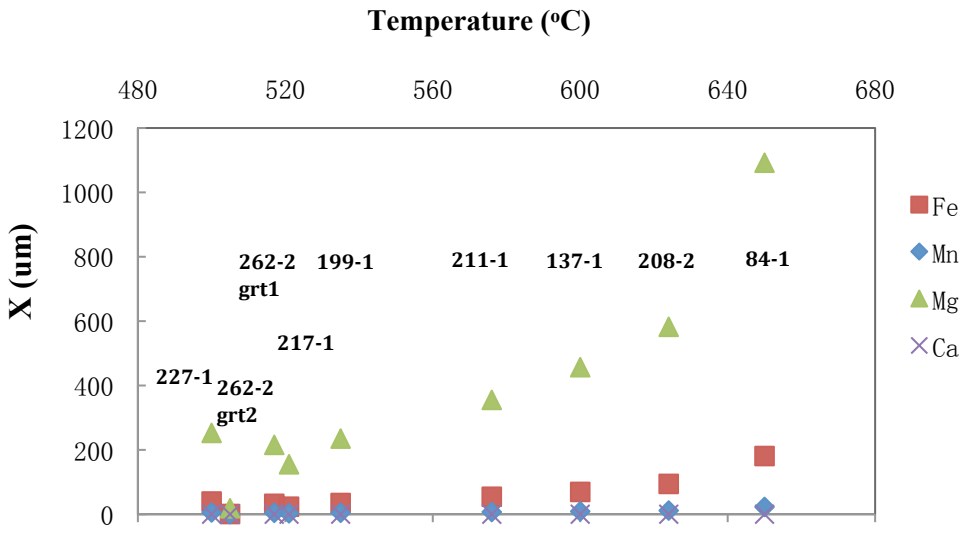

Figure 12 Diffusion distances of 2^+ cations. Calculated with t= 45 Ma

By examining the widths of inclusion-poor overgrowths on garnets, time scales that would be necessary to achieve diffusive equilibration of the overgrowths can be calculated by inverting equation [2] (Appendix IV). For each garnet, the width of the widest overgrowth was selected for x. The times that would be necessary to obtain the overgrowths by diffusion would be 1.04×10^5 Ma to 2.91 Ma for Fe, 7.07×10^5 Ma to 1.86×10^2 Ma for Mn, 1.67×10^2 Ma to 0.08 Ma for Mg, and 1.91×10^{11} Ma to 7.07×10^7 Ma for Ca.

These two sets of calculations demonstrate that the zoning in the Black Hills garnets cannot be the results of diffusive equilibration during contact metamorphism by the HPG, particularly for Ca. There simply was not sufficient time for appreciable equilibration by diffusion to occur. Diffusion of Fe, Mg and Mn could have modified garnet zoning only partially to give smoothed zoning profiles shown by the X-ray maps. The time scales for the diffusion of Ca are too long to have affected its zoning. In the X-ray maps, Ca zoning always defines interior dodecahedral shapes of garnets. The Ca zoning in the Black Hills supports the contention of Spear and Daniel (2001) that Ca zoning is diffusion-controlled. X-ray maps demonstrate that the diffusion of Y was also negligible.

According to Carlson (2002) and Meth and Carlson (2005), Fe, Mg and Mn reach rock-wide equilibrium by intergranular diffusion in greenschist facies conditions over metamorphic time scales. However, integranular diffusion of Ca is too slow for rock-scale equilibrium below upper amphibolite facies conditions. Thus, zoning of Fe, Mg and Mn in our garnets reflects the changing P-T conditions during garnet growth. However, internal equilibration in garnet was not attained in the garnet and staurolite zones, and this needs to be further discussed.

Disequilibrium versus equilibrium garnet growth

Morphologically, there are mainly two types of garnets in Black Hills schists. One type is the inclusion-rich garnet, with or without inclusion-free overgrowth. Some of the inclusion-rich cores have features that suggest radial growth (Figure 3c, e, g). The other type is garnet that is inclusion-poor. The presence of inclusions and radial growth features in the first garnet type suggest disequilibrium growth. This can be evaluated by

comparison of apparent growth temperatures with predicted equilibrium temperatures. The volume percent isopleths of garnet show that garnet should have started growing in the metapelites at approximately 400°C (Figure 13). However, the apparent temperatures for initial garnet growth are >450°C. This suggests that the equilibrium temperature of garnet growth was overstepped (Wilbur and Augue, 2006).

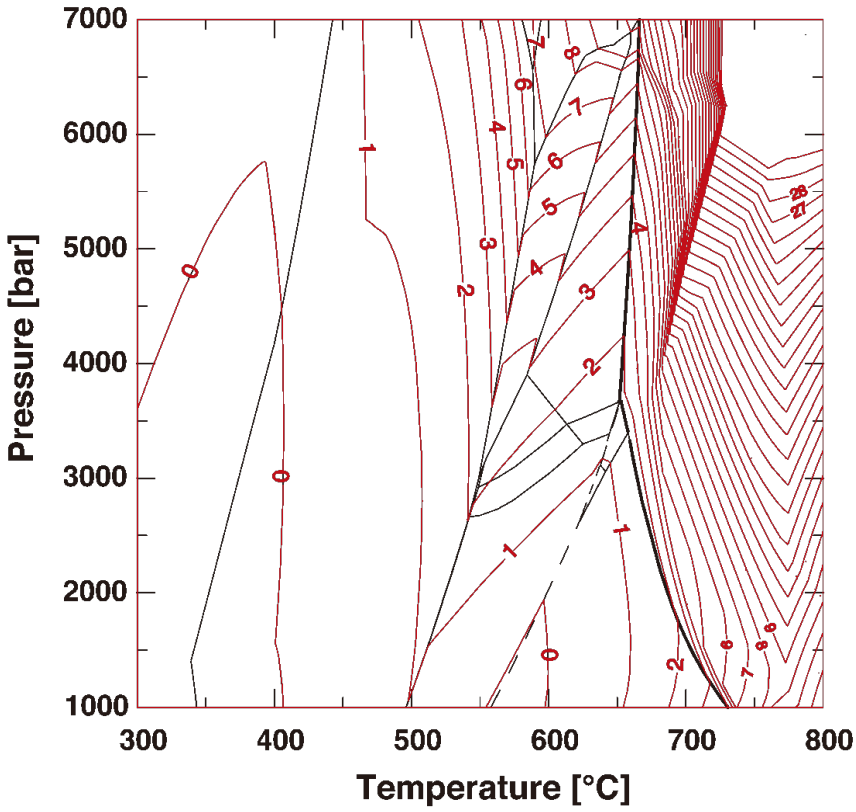

Figure 13 Isopleths of volume % of garnet calculated by THERIAK-DOMINO for a(H_2O)=1

The overstepping of the equilibrium nucleation temperature and the presence of radially-distributed inclusions may be related to low a(H_2O) conditions in the rocks (Huff and Nabelek, 2006), that would have reduced the intergranular diffusivity of the essential components necessary for garnet growth, particularly that of Al (Carlson, 2005).

Nevertheless, the growth rates of garnets were faster than the rates of inclusion removal in the low a(H_2O) environment. Moreover, Y concentrations are generally high in cores, indicated that garnets had only one nucleation site and does not support a coalescence of multiple nuclei as suggested by Spear and Daniel (1998) for garnets in Harpswell Neck, Maine. The inclusion-free overgrowths on the inclusion-rich cores reflect a slower crystallization related to hydrothermal activity associated with emplacement of the HPG that is evident in post-kinematic growth of chlorite. Compositions of the overgrowths give temperatures that are consistent with the metamorphic grade achieved by the host rocks.

Close to the HPG in the sillimanite zone, intergranular diffusivity was fast enough to remove inclusions while the garnets grew. In the sillimanite zone, garnets do not preserve an early metamorphic history of the host rocks. It appears that the garnets fully recrystallized from low-grade garnets in a higher T and higher a(H_2O) environment. They are compositionally uniform and compositions appear to reflect the pressure and temperature achieved by the rocks. Zoning of Ca, Mg, Mn and Y on rims (Figure 11, 12) may have been caused by retrograde metamorphism associated with fluid influx and decompression (Figure 4h, 10i).

P-T-t paths

A previous study of the pressure and temperature condition in the Black Hills by Helm and Labtka (1991) proposed that the metamorphic terrain around the HPG had a low-pressure and high-temperature history. The P-T-t path for the Bear Mountain region (Figure 2) constructed by Dahl et al. (2005b) by combination of microstructure, petrology and microchronometry shows relatively high-P metamorphism during D_2 between ~1775

and 1750 Ma. Calculated pressures and temperatures in this research indicate an increase from the garnet zone to the sillimanite zone. However, the indicated P-T-t paths in the various parts of the Proterozoic terrain are different.

For most garnets in the garnet zone, indicated pressure ranges are more remarkable than temperature ranges (Figure 10a-d). Hence, the host metamorphic rocks (Figure 1) may have experienced continued burial while garnet cores crystallized during the regional metamorphism beginning at ~1750 Ma until ~1715 Ma (M_2). The temperature increase suggested by compositions of rims might be due to heating by intrusion of leucogranites in the northern Black Hills that is evident by their presence in recovered drill cores and near the town of Tilton (Figure 1).

The P-T-t paths indicated by garnets near the staurolite isograd display well the transition from M_2 to M_3 (Figure 10e, f). Temperature apparently increased during growth of overgrowths on garnets. It indicates the reheating and increase of H_2O activity in the upper garnet and staurolite zones during HPG intrusion.

Samples from the sillimanite zone record a high-P and high-T history (Figure 10i), with pressure in excess of 5 kbar. The high pressure is consistent with the noted occurrence of kyanite in the sillimanite zone but is inconsistent with the low-P and high-T metamorphism proposed by Helms and Labotka (1991). Except for the evidence in the garnets and the one remnant occurrence of kyanite, other indications of high pressures were mostly wiped out with continued hydrothermal activity during the uplift of the HPG block between the Keystone and Hill City faults (Nabelek et al., 2006). Rims of the garnets in the sillimanite zone record a decrease in pressure and temperature, that

eventually reached the andalusite stability field as evidenced by occurrences of andalusite in the high-strain aureole of the HPG.

Conclusions

Garnet growth and zoning in the Black Hills was diffusion-limited. Garnet compositions reflect evolution of P-T conditions and fluid compositions. In the garnet and staurolite zones, garnets mostly have large inclusions-rich cores and almost inclusion-free overgrowth. They started growing in a low a(H_2O) environment by overstepping of the equilibrium crystallization temperature during the regional metamorphism caused by the collision of Wyoming and Superior cratons. The overgrowths grew in the presence of aqueous fluids during heating associated with granite emplacement in the region and perhaps some decompression.

With increase in metamorphic grade, most garnets contain fewer inclusions. They partially or fully recrystallized in a higher a(H_2O) condition that accompanied heating from the HPG. Compositions of garnet in the sillimanite zone suggest that pressure may have reached at least 5 kbar. However, as retrograde metamorphism occurred, rims record lower P and T conditions that reflect decompression of the region between the Keystone and Hill City faults.

Reference

Anderson, D. E. & Buckley, G. R., 1973. Zoning in garnets: Diffusion models. Contribution to Mineralogy and Petrology, **40**, 87-104.

Berman R.G. & Brown T.H., 1984. A thermodynamic model for multicomponent melts, with application to the system CaO-Al2O3-SiO2. Geochim. Cosmochim, Acta, **48**, 661-678.

Berman, R.G., 1991. Thermobarometry using multi-equilibrium calculations: a new technique, with petrological applications. Canadian Mineralogist, **29**, 833-855.

Capitani, C.D. & Petrakakis, K., 2010. THERIAK-DOMINO user's guide, vers. 01.08.09.

Carlson, W. D., 2010. Dependence of reaction kinetics on H_2O activity as inferred from rates of intergranular diffusion of aluminium. Metamorphic Geology, 28, 735-752.

Carlson, W. D., 2006. Rates of Fe, Mg, Mn, and Ca diffusion in garnet. American Mineralogist, **91**, 1-11.

Carlson, W. D., 2002. Scales of disequilibrium and rates of equilibration during metamorphism. American Mineralogist, **87**, 185-204.

Crank, J., 1975. The Mathematics of Diffusion. Oxford University Press, New York, 452 p.

Cygan, R. T. & Lasaga, A. C., 1982. Crystal growth and the formation of chemical zoning in garnets. Contributions to mineralogy and petrology, **79**, 187-200.

Dahl, P.S., Frei, R. & Dorais, M.J., 1998. When did the Wyoming Province collide with Laurentia? New clues from step-leach Pb-Pb dating of garnet independent of its inclusions. Geological Society of America Abstracts with Programs, **30(7)**, 109.

Dahl, P.S., Holm, D.K., Gardner, E.T., Hubacher, F.A. & Foland, K.A., 1999. New constraints on the timing of Early Proterozoic tectonism in the Black Hills (SD), with implications for the docking of the Wyoming province with Laurentia. Geological Society of America Bulletin, **111**, 1335-1349.

Dahl, P. S., Hamilton, M. A. Jercinovic, M. J., Terry, M. P., Williams, M. L. & Frei, R., 2005a. Comparative isotopic and chemical geochronology of monazite, with implications

for U-Th-Pb dating by electron microprobe: An example from metamorphic rocks of the eastern Wyoming Craton (U.S.A). American Mineralogist, **90**, 619-638

Dahl, P. S., Terry, M. P., Jercinovic, M. J., Willians, M. L., Hamilton, M. A., Foland, K. A., Clement, S. M. & Friberg, L. M., 2005b. Electron probe (Ultrachron) microchronometry of metamorphic monazite: Unraveling the timing of polyphase thermotectonism in the easternmost Wyoming Craton (Black Hills, South Dakota). American Mineralogist, **90**, 1712-1728.

Daniel, C. G. & Spear, F. S., 1999. The clustered nucleation and growth processes of garnet in regional metamorphic rocks from north-west Connecticut, USA. Metamorphic Geology, **17**, 503-520.

Daniel, C. G. & Spear, F. S., 1998. Three-dimensional patterns of garnet nucleation and growth. Geology, **26**, 503-506.

De Capitani, C. & Petrakakis, K., 2010. The computation of equilibrium assemblage diagrams with Theriak/Domino software. American Mineralogist, **95**, 1006-1016.

Deer, W. A., Howie, R. A. & Zussman, J., 1992. An introduction to the rock-forming minerals-2nd ed., British library cataloguing in publication data.

DeYoreo, J.J., Lux, D.R. & Guidotti, C.V., 1991. Thermal modeling in low-pressure/high-temperature metamorphic belts. Tectonophysics, 188, 209-238.

Duke, E. F., Redden, J. A. & Papike, J. J., 1988. Calamity Peak layered granite-pegmatite complex, Black Hills, South Dakota: Part I. Structure and emplacement. Geological Society of America Bulletin, **100**, 825-840.

Duke, E. F., 1995. Contrasting scales of element mobility in metamorphic rocks near Harney Peak Granite, Black Hills, South Dakota. Geological Society of America Bulletin, **107**, 274-285.

Duke, E. F., 1996. Geochemistry of lower Proterozoic metagraywack, Black Hills, South Dakota- Regional and outcrop-scale variations. in Paterson, C. J., and Kirchner, J. G., eds., Guidebook to the geology of the Black Hills: South Dakota School of Mines and Technology Bulletin no. **19**,180-190.

England, P.C. & Thompson, A.B., 1986. Some thermal and tectonic models for crustal melting in continental collisional zones. In M.P. Coward and A.C. Ries, Eds., Collisional Tectonics, Geological Society of London Special Publication **19**, 83-94.

Friberg, L.M., Dahl, P.S. & Terry, M.P., 1996. Thermotectonic evolution of Early Proterozoic metamorphic rocks from the southern Black Hills, South Dakota. South Dakota School of Mines Bulletin, **19**, 191-199.

Helms, T.S. & Labotka, T.C., 1991. Petrogenesis of Early Proterozoic pelitic schists of the southern Black Hills, South Dakota: Constrains on regional low-pressure metamorphism. Geological Society of America Bulletin, **103**, 1324-1334.

Hickmott, D. D., Shimizu, N., Spear, F. S. & Selverstone, J., 1987. Geology, **15**, 573-576.
Hickmott, D. D. & Spear, F. S., 1992. Major-and trace-element zoning in garnet from calcareous pelites in the NW Shelburne Falls Quadrangle, Massachusetts: Garnet growth histories in retrograded rocks. Journal of Petrology, **33**, 965-1005.

Hill, J., Nabelek, P. I. & Bauer, R., 2004. Differential deformational history of fault-bounded blocks: "Southern Trans-Hudson" orogen, Black Hills, South Dakota. Geological Society of America Abstracts with programs, 36, 569.

Holm, D.K., Dahl, P.S. & Lux, D.R., 1997. $^{40}Ar/^{39}Ar$ evidence for Middle Proterozoic (1300-1500) slow cooling of the southern Black Hills, South Dakota: Implications for Proterozoic P-T evolution and post-tectonic magmatism. Tectonics, **16**, 609-622.

Holland, T.J.B & Powell, R., 1998. An internally consistent thermodynamic data set for phases of petrological interest. Journal of Metamorphic Geolgy, **16**, 309-343.

Huff, A. T. & Nabelek, P.I., 2007. Production of carbonic fluids during metamorphism of graphitic pelites in a collisional orogen - An assessment from fluid inclusions, Geochimica et Cosmochimica Acta, **71**, 4997-5015.

Krogstad, E.J. & Walker, R.J., 1994. High closure temperatures of the U-Pb system in large apatites from the Tin Mountain pegmatite, Black Hills, South Dakota. USA. Geochimica et Cosmochimica Acta, **58**, 3845-3853.

Meth, C. E. & Carlson, W. D., 2005. Diffusion-controlled synkinematic growth of garnet from a heterogeneous precursor at Passo del Sole, Switzerland. The Canadian Mineralogist, **43**, 157-182.

Nabelek P. I. & Ternes K., 1997. Fluid inclusions in the Harney Peak Granite, Black Hills, South Dakota, USA: Implications for solubility and evolution of magmatic volatiles and crystallization of leucogranite magmas. Geochim. Cosmochim. Acta, **61**, 1447–1465.

Nabelek P. I., 1997. Quartz-sillimanite leucosomes in high-grade schists, Black Hills, South Dakota: A perspective on the mobility of Al in high-grade metamorphic rocks. geology, **25**, 995-998.

Nabelek P. I., 1999. Trace-element distribution among rock-forming minerals in Black Hills migmatites, South Dakota: a case for solid-state equilibrium. American Minerologist, **84**, 1256-1269.

Nabelek, P.I., Liu, M. & Sirbescu, M., 2001. Thermo-rheological, shear heating model for leucogranite generation, metamorphism, and deformation during the Proterozoic Trans-Hudson orogeny, Black Hills, South Dakota. Tectonophysics, **342**, 371-388.

Nabelek P. I., Wilke M., Huff T. A. & Wopenka B., 2003. Methane, an important component of fluids in graphitic metapelites. Geochim. Cosmochim. Acta, **67**, A317.
Nabelek, P.I., Labotka, T.C., Helms, T. & Wilke, M., 2006. Fluid mediated polymetamorphism related to Proterozoic collision of Archean Wyoming and Superior provinces in the Black Hills, South Dakota. American Mineralogist, **91**, 1473-1487.

Philpotts A. R. & Ague J. J., 2009. Principles of Igneous and Metamorphic Petrology. United States of America by Cambridge University Press, New York, 563p.

Redden, J. A. and DeWitt, E., 2008. Maps showing geology structure, and geophysics of the central Black Hills, South Dakota. Scientific Investigations map 2777.

Redden, J. A., Peterman, Z. E., Zartman, R. E., & DeWitt, E., 1990. U-Th-Pb zircon and monazite ages and preliminary interpretation of the tectonic development of Precambrian rocks in the Black Hills. In J. F. Lewry and M. R. Stauffer, Eds., The early Proterozoic Trans-Hudson Orogeny of North America. Geological association of Canada Special Paper, **37**, 229-251.

Redden, J. A. & Norton, J. J., 1992. Alkali and related metasomatism during thermal metasomatism around the Harney Peak Granite, Black Hills, South Dakota. Geological Society of America Abstracts with Programs, **24**, 58.

Schwandt, C.S., Cygan, R.T. & Westrich, H.R., 1995. Mg self-diffusion in pyrope garnet. American Mineralogist, **80**, 483–490.

Schwandt, C.S., Cygan, R.T. & Westrich, H.R., 1996a. Ca self-diffusion in grossular garnet. American Mineralogist, **81**, 448–451.

Schwandt, C. S., Papike, J. J., & Shearer, C. K., 1996b. Trace element zoning in pelitic garnet of the Black Hills, South Dakota, American Mineralogist, **81**, 1195-1207.

Shearer, C. K., Papike, J. J., Redden, J. A., Simon, S., Walker, R. J., & Laul, J.C., 1987. Origin of pegmatitc granite segregation, Willow Creek, Black Hills, South Dakota. Canadian Mineralogist, **25**, 159-171.

Spear, F. S. & Pyle, J.M., 2010. Theoretical modeling of monazite growth in a low-Ca metapelite. Chemical Geology, **273**, 111-119.

Spear, F. S. & Daniel, C. G., 2001. Diffusion control of garnet growth, Harpswell Neck, Maine, USA. Metamorphic Geology, **19**, 179-195.

Spear, F. S. & Kohn, M. J., 1996. Trace element zoning in garnet as a monitor of crustal melting. Geology, **24**, 1099-1102.

Spear, F.S. & Selverstone, J., 1983. Quantitative P-T path from zoned minerals: theory and tectonic applications. Contributions to Mineralogy and Petrology, **83**, 348–357.

Stone, R.E., 2005. Causes of incipient garnet growth in garnet-biotite grade pelitic schists, the Black Hills, South Dakota. 45p. M.S. Thesis, University of Missouri, Columbia.

Terry, M.P. & Friberg, L.M., 1990. Pressure-temperature-time path related to the thermotectonic evolution of an Early Proterozoic metamorphic terrane, Black Hills, South Dakota. Geology, **18**, 786-789.

Vance, D. & Mahar, E., 1998. Pressure-temperature paths from P-T pseudosections and zoned garnets; potential, limitations and examples from the Zanskar Himalaya, NW India. Contributions to Mineralogy and Petrology, **132**, 225–245.

Wilbur D. E. & Ague J. J., 2006. Chemical disequilibrium during garnet growth: Monte Carlo simulations of natural crystal morphologies, Geological Society of America, **34**, 689-692.

Wilke M., Nabelek P. I. & Glascock M. D., 2002. B and Li in metapelites from the Proterozoic Terrane in the Black Hills, South Dakota, USA: Implications for the origin of leucogranitic magmas. American Mineralogist, 87, 491–500.

Williams, M.L. & Karlstrom, K.E., 1996. Looping P-T paths, high-T, low-P middle crustal metamorphism: Proterozoic evolution of the southwestern United States. Geology, **24**, 1119-1122.

Appendix I

Table of microprobe compositional analysis data for all samples

SAMPLE	Na	Mg	Al	Si	K	Ca	Mn	Fe	Ti	Cr	Zr	Y
217-1	0.006	0.104	2.014	2.983	0.001	0.211	0.871	1.814	0.003	0.000	0.000	0.001
217-1	0.032	0.103	2.013	2.981	0.003	0.236	0.891	1.762	0.002	0.001	0.000	0.001
217-1	0.001	0.096	2.016	2.980	0.000	0.271	0.923	1.715	0.004	0.000	0.000	0.001
217-1	0.004	0.090	2.013	2.985	0.000	0.277	0.981	1.646	0.006	0.001	0.000	0.001
217-1	0.026	0.078	2.011	2.978	0.002	0.323	1.070	1.528	0.005	0.002	0.000	0.001
217-1	0.009	0.077	1.997	2.996	0.000	0.344	1.070	1.489	0.007	0.001	0.000	0.008
217-1	0.006	0.084	2.020	2.974	0.001	0.271	1.104	1.528	0.006	0.002	0.000	0.011
217-1	0.004	0.082	2.024	2.973	0.000	0.279	1.102	1.528	0.006	0.000	0.000	0.009
217-1	0.002	0.079	2.022	2.971	0.000	0.315	1.115	1.486	0.008	0.000	0.000	0.007
217-1	0.005	0.078	2.019	2.969	0.000	0.305	1.132	1.490	0.007	0.000	0.000	0.008
217-1	0.004	0.080	2.022	2.968	0.000	0.300	1.133	1.491	0.007	0.000	0.000	0.008
217-1	0.001	0.079	2.008	2.984	0.001	0.272	1.136	1.502	0.008	0.002	0.000	0.006
217-1	0.004	0.080	2.012	2.977	0.000	0.288	1.117	1.516	0.009	0.002	0.000	0.003
217-1	0.004	0.080	1.979	2.993	0.000	0.320	1.110	1.509	0.010	0.002	0.000	0.002
217-1	0.008	0.080	1.999	2.989	0.000	0.276	1.101	1.523	0.004	0.001	0.000	0.020
217-1	0.010	0.077	1.988	2.994	0.001	0.345	1.069	1.512	0.008	0.000	0.000	0.003
217-1	0.003	0.078	1.994	2.994	0.000	0.323	1.050	1.551	0.006	0.001	0.000	0.002
217-1	0.006	0.085	1.985	2.995	0.001	0.282	1.013	1.629	0.005	0.001	0.000	0.005
217-1	0.010	0.094	1.992	2.995	0.001	0.232	0.943	1.734	0.004	0.001	0.000	0.003

SAMPLE	Na	Mg	Al	Si	K	Ca	Mn	Fe	Ti	Cr	Zr	Y
217-1	0.006	0.106	1.992	2.994	0.001	0.195	0.882	1.827	0.003	0.002	0.000	0.001
262-2 grt1	0.002	0.112	1.999	3.000	0.001	0.277	0.980	1.621	0.003	0.001	0.000	0.000
262-2 grt1	0.003	0.106	1.995	2.998	0.000	0.341	1.017	1.535	0.005	0.001	0.000	0.000
262-2 grt1	0.001	0.089	1.994	2.999	0.001	0.406	1.076	1.427	0.005	0.001	0.000	0.000
262-2 grt1	0.002	0.073	1.990	2.993	0.001	0.431	1.197	1.308	0.009	0.000	0.000	0.000
262-2 grt1	0.028	0.079	1.988	2.991	0.001	0.303	1.217	1.402	0.008	0.002	0.000	0.000
262-2 grt1	0.004	0.083	1.978	2.995	0.000	0.266	1.234	1.437	0.010	0.001	0.000	0.000
262-2 grt1	0.004	0.079	1.971	3.009	0.001	0.315	1.204	1.409	0.008	0.000	0.000	0.000
262-2 grt1	0.002	0.084	1.977	3.002	0.000	0.273	1.259	1.387	0.008	0.001	0.000	0.005
262-2 grt1	0.003	0.082	1.959	3.006	0.000	0.262	1.296	1.375	0.013	0.000	0.001	0.003
262-2 grt1	0.003	0.089	1.975	3.001	0.000	0.256	1.309	1.356	0.005	0.000	0.000	0.010
262-2 grt1	0.002	0.079	1.958	3.006	0.001	0.289	1.293	1.361	0.012	0.000	0.000	0.002
262-2 grt1	0.001	0.078	1.975	2.993	0.000	0.307	1.267	1.382	0.007	0.000	0.000	0.001
262-2 grt1	0.000	0.079	1.982	2.993	0.000	0.303	1.252	1.391	0.007	0.000	0.000	0.001
262-2 grt1	0.002	0.085	1.965	2.996	0.000	0.298	1.218	1.438	0.009	0.000	0.000	0.000
262-2 grt1	0.002	0.079	1.974	2.989	0.000	0.279	1.238	1.444	0.010	0.001	0.000	0.000
262-2 grt1	0.001	0.070	1.970	2.979	0.001	0.443	1.219	1.334	0.010	0.000	0.000	0.000
262-2 grt1	0.002	0.072	1.970	2.990	0.000	0.442	1.188	1.347	0.006	0.001	0.000	0.000
262-2 grt1	0.000	0.085	1.970	2.984	0.001	0.446	1.116	1.414	0.007	0.000	0.000	0.000

SAMPLE	Na	Mg	Al	Si	K	Ca	Mn	Fe	Ti	Cr	Zr	Y
262-2 grt1	0.001	0.097	1.983	2.968	0.000	0.414	1.059	1.504	0.005	0.001	0.000	0.000
262-2 grt1	0.002	0.113	1.991	2.971	0.001	0.311	1.003	1.635	0.003	0.001	0.000	0.000
262-2 grt2	0.001	0.106	1.990	3.005	0.002	0.279	1.029	1.582	0.002	0.001	0.000	0.001
262-2 grt2	0.002	0.101	1.972	3.006	0.000	0.367	1.052	1.496	0.005	0.001	0.000	0.001
262-2 grt2	0.003	0.104	1.970	3.009	0.001	0.345	1.145	1.414	0.004	0.000	0.000	0.006
262-2 grt2	0.000	0.093	1.975	3.003	0.000	0.267	1.213	1.435	0.010	0.001	0.000	0.000
262-2 grt2	0.004	0.089	1.977	3.005	0.000	0.263	1.222	1.434	0.007	0.000	0.000	0.000
262-2 grt2	0.005	0.063	1.900	3.114	0.001	0.233	1.208	1.385	0.014	0.001	0.000	0.001
262-2 grt2	0.006	0.060	1.945	2.961	0.005	0.230	1.210	1.491	0.080	0.001	0.001	0.001
262-2 grt2	0.006	0.057	1.836	3.208	0.002	0.225	1.177	1.341	0.011	0.002	0.000	0.002
262-2 grt2	0.005	0.073	1.963	3.039	0.002	0.235	1.215	1.433	0.008	0.001	0.000	0.002
262-2 grt2	0.002	0.070	1.922	3.103	0.000	0.231	1.189	1.405	0.007	0.001	0.000	0.001
262-2 grt2	0.003	0.071	1.903	3.130	0.001	0.229	1.174	1.392	0.007	0.001	0.000	0.001
262-2 grt2	0.004	0.076	1.963	3.067	0.000	0.250	1.173	1.396	0.011	0.001	0.000	0.000
262-2 grt2	0.002	0.091	1.990	2.995	0.000	0.248	1.213	1.450	0.009	0.001	0.001	0.001
262-2 grt2	0.003	0.094	1.986	2.993	0.001	0.242	1.216	1.459	0.010	0.001	0.000	0.000
262-2 grt2	0.004	0.091	1.984	2.995	0.000	0.260	1.211	1.446	0.012	0.001	0.000	0.000
262-2 grt2	0.004	0.102	1.975	2.985	0.001	0.300	1.190	1.449	0.012	0.000	0.000	0.000
262-2 grt2	0.004	0.082	1.666	3.471	0.000	0.322	0.925	1.219	0.003	0.001	0.000	0.001

SAMPLE	Na	Mg	Al	Si	K	Ca	Mn	Fe	Ti	Cr	Zr	Y
262-2 grt2	0.003	0.107	1.989	2.992	0.000	0.376	1.056	1.476	0.005	0.001	0.000	0.003
262-2 grt2	0.002	0.102	1.984	3.007	0.001	0.287	1.036	1.572	0.004	0.001	0.000	0.002
211-1	0.003	0.156	1.995	3.010	0.001	0.350	0.299	2.173	0.002	0.002	0.000	0.001
211-1	0.001	0.142	1.997	3.006	0.000	0.363	0.710	1.769	0.004	0.000	0.000	0.001
211-1	0.000	0.119	1.998	3.006	0.000	0.354	0.896	1.611	0.005	0.000	0.000	0.001
211-1	0.000	0.112	1.990	3.009	0.000	0.334	0.959	1.578	0.006	0.000	0.000	0.000
211-1	0.000	0.106	1.994	3.007	0.000	0.332	0.998	1.545	0.006	0.001	0.000	0.001
211-1	0.001	0.103	1.993	3.010	0.000	0.315	1.031	1.528	0.006	0.000	0.000	0.000
211-1	0.000	0.115	1.991	3.011	0.000	0.306	1.048	1.508	0.007	0.001	0.000	0.000
211-1	0.002	0.117	1.994	3.003	0.000	0.314	1.048	1.512	0.006	0.000	0.000	0.000
211-1	0.003	0.111	2.001	3.003	0.000	0.314	1.047	1.508	0.005	0.000	0.000	0.000
211-1	0.001	0.109	1.999	3.010	0.000	0.309	1.042	1.507	0.006	0.000	0.000	0.000
211-1	0.001	0.112	1.998	3.001	0.000	0.325	1.036	1.514	0.006	0.000	0.000	0.000
211-1	0.000	0.116	2.003	3.004	0.000	0.319	1.031	1.509	0.006	0.000	0.000	0.000
211-1	0.001	0.119	1.999	3.005	0.000	0.336	1.017	1.506	0.006	0.001	0.000	0.000
211-1	0.000	0.123	1.997	3.008	0.000	0.342	0.939	1.569	0.007	0.001	0.000	0.001
211-1	0.002	0.124	2.005	2.996	0.000	0.378	0.884	1.603	0.005	0.001	0.000	0.000
211-1	0.001	0.132	2.011	2.992	0.000	0.427	0.760	1.674	0.002	0.001	0.000	0.000
211-1	0.001	0.200	2.005	3.001	0.000	0.208	0.484	2.094	0.000	0.001	0.000	0.001

SAMPLE	Na	Mg	Al	Si	K	Ca	Mn	Fe	Ti	Cr	Zr	Y
211-1	0.003	0.217	2.008	2.997	0.000	0.149	0.394	2.230	0.001	0.000	0.000	0.000
211-1	0.003	0.218	2.012	2.994	0.001	0.130	0.306	2.332	0.000	0.002	0.000	0.002
211-1	0.001	0.118	1.992	3.019	0.000	0.355	0.960	1.530	0.005	0.000	0.000	0.000
211-1	0.002	0.124	1.996	3.005	0.000	0.321	1.052	1.486	0.006	0.000	0.000	0.000
211-1	0.002	0.155	1.995	3.004	0.000	0.425	0.578	1.833	0.002	0.002	0.000	0.000
208-2	0.003	0.217	2.002	3.001	0.001	0.064	0.242	2.467	0.001	0.002	0.000	0.000
208-2	0.001	0.267	1.996	2.995	0.000	0.080	0.306	2.359	0.001	0.001	0.000	0.001
208-2	0.000	0.243	1.999	2.992	0.001	0.109	0.413	2.247	0.001	0.000	0.000	0.000
208-2	0.000	0.217	1.994	2.989	0.000	0.162	0.518	2.117	0.007	0.000	0.000	0.001
208-2	0.000	0.185	1.994	2.993	0.000	0.236	0.632	1.963	0.002	0.001	0.000	0.001
208-2	0.000	0.161	1.996	2.993	0.000	0.270	0.735	1.844	0.004	0.000	0.000	0.001
208-2	0.001	0.141	1.989	2.994	0.000	0.290	0.833	1.750	0.005	0.001	0.000	0.000
208-2	0.001	0.119	1.989	2.999	0.000	0.309	0.930	1.649	0.006	0.000	0.000	0.000
208-2	0.002	0.106	1.996	2.988	0.000	0.318	1.010	1.581	0.006	0.000	0.000	0.002
208-2	0.009	0.111	1.996	2.990	0.000	0.271	1.037	1.551	0.004	0.001	0.000	0.027
208-2	0.009	0.110	1.998	2.989	0.000	0.265	1.036	1.554	0.005	0.000	0.000	0.029
208-2	0.007	0.107	1.994	2.998	0.000	0.272	1.039	1.543	0.005	0.001	0.000	0.024
208-2	0.005	0.106	1.993	2.997	0.001	0.280	1.038	1.550	0.007	0.001	0.000	0.015
208-2	0.004	0.107	1.986	3.004	0.001	0.292	1.030	1.553	0.006	0.001	0.000	0.010

SAMPLE	Na	Mg	Al	Si	K	Ca	Mn	Fe	Ti	Cr	Zr	Y
208-2	0.000	0.117	1.993	2.994	0.000	0.309	0.952	1.631	0.006	0.000	0.000	0.001
208-2	0.000	0.137	1.994	2.994	0.000	0.296	0.843	1.733	0.005	0.000	0.000	0.001
208-2	0.001	0.153	1.988	2.999	0.000	0.273	0.769	1.818	0.003	0.001	0.000	0.001
208-2	0.002	0.195	2.004	2.991	0.000	0.195	0.600	2.013	0.002	0.002	0.000	0.002
208-2	0.000	0.233	1.999	2.999	0.000	0.110	0.473	2.185	0.001	0.000	0.000	0.000
208-2	0.001	0.258	2.002	2.995	0.000	0.078	0.327	2.341	0.001	0.000	0.000	0.000
208-2	0.002	0.259	2.009	2.990	0.000	0.066	0.266	2.413	0.000	0.001	0.000	0.000
208-2	0.005	0.230	2.007	2.991	0.001	0.062	0.241	2.470	0.000	0.001	0.000	0.000
199-1	0.003	0.167	2.017	2.971	0.001	0.170	0.704	1.986	0.000	0.001	0.000	0.000
199-1	0.003	0.208	2.001	2.972	0.001	0.193	0.665	1.977	0.003	0.001	0.000	0.000
199-1	0.003	0.196	2.007	2.970	0.000	0.208	0.666	1.968	0.003	0.001	0.001	0.000
199-1	0.003	0.184	1.998	2.970	0.000	0.213	0.677	1.971	0.008	0.001	0.000	0.000
199-1	0.003	0.159	2.010	2.966	0.000	0.217	0.693	1.966	0.008	0.001	0.000	0.000
199-1	0.001	0.179	2.000	2.967	0.000	0.214	0.686	1.970	0.007	0.001	0.000	0.000
199-1	0.002	0.150	2.001	2.962	0.000	0.206	0.709	1.997	0.004	0.001	0.000	0.002
199-1	0.003	0.141	2.012	2.965	0.000	0.172	0.729	1.999	0.002	0.000	0.000	0.004
199-1	0.003	0.131	2.013	2.964	0.001	0.170	0.747	1.985	0.004	0.001	0.000	0.005
199-1	0.003	0.150	2.009	2.963	0.002	0.208	0.702	1.981	0.005	0.001	0.000	0.001
199-1	0.003	0.162	1.994	2.963	0.000	0.195	0.697	2.002	0.012	0.001	0.000	0.000

SAMPLE	Na	Mg	Al	Si	K	Ca	Mn	Fe	Ti	Cr	Zr	Y
199-1	0.002	0.147	2.013	2.961	0.001	0.225	0.709	1.967	0.005	0.000	0.000	0.001
199-1	0.004	0.189	2.011	2.954	0.000	0.223	0.672	1.973	0.007	0.001	0.000	0.000
199-1	0.002	0.183	2.008	2.953	0.000	0.255	0.672	1.958	0.005	0.000	0.000	0.000
199-1	0.001	0.171	1.992	2.967	0.000	0.210	0.692	1.992	0.005	0.001	0.000	0.000
199-1	0.004	0.189	2.002	2.957	0.001	0.232	0.669	1.981	0.004	0.001	0.000	0.000
199-1	0.003	0.183	1.935	3.049	0.001	0.213	0.662	1.926	0.006	0.001	0.000	0.000
199-1	0.003	0.152	1.943	3.042	0.001	0.185	0.694	1.951	0.007	0.001	0.000	0.000
199-1	0.001	0.184	2.002	2.957	0.001	0.214	0.689	1.984	0.004	0.002	0.000	0.000
199-1	0.003	0.200	2.003	2.962	0.000	0.230	0.665	1.966	0.004	0.001	0.000	0.000
199-1	0.006	0.211	2.002	2.980	0.004	0.183	0.650	1.982	0.003	0.000	0.000	0.000
199-1	0.001	0.194	2.011	2.961	0.000	0.185	0.680	1.999	0.001	0.000	0.000	0.000
227-1	0.002	0.062	2.013	2.994	0.001	0.346	1.273	1.300	0.004	0.000	0.000	0.001
227-1	0.001	0.070	2.004	2.990	0.000	0.391	1.186	1.355	0.005	0.001	0.000	0.000
227-1	0.000	0.067	2.005	2.991	0.000	0.353	1.249	1.330	0.005	0.000	0.000	0.000
227-1	0.007	0.069	2.002	2.992	0.000	0.319	1.283	1.326	0.006	0.001	0.000	0.000
227-1	0.001	0.067	2.002	2.996	0.000	0.311	1.305	1.309	0.006	0.000	0.000	0.000
227-1	0.002	0.063	1.979	3.026	0.000	0.263	1.333	1.305	0.006	0.001	0.000	0.000
227-1	0.001	0.065	1.971	3.038	0.000	0.242	1.346	1.300	0.006	0.001	0.000	0.000
227-1	0.073	0.069	1.974	3.003	0.045	0.250	1.344	1.275	0.017	0.000	0.000	0.001

SAMPLE	Na	Mg	Al	Si	K	Ca	Mn	Fe	Ti	Cr	Zr	Y
227-1	0.002	0.069	1.702	3.429	0.000	0.205	1.175	1.123	0.006	0.000	0.000	0.002
227-1	0.002	0.071	1.975	3.034	0.001	0.239	1.356	1.282	0.007	0.000	0.000	0.003
227-1	0.002	0.072	2.001	2.995	0.000	0.247	1.374	1.292	0.008	0.000	0.000	0.003
227-1	0.000	0.070	2.003	2.997	0.000	0.251	1.369	1.296	0.007	0.000	0.000	0.000
227-1	0.002	0.070	2.009	2.989	0.001	0.252	1.363	1.306	0.008	0.000	0.000	0.000
227-1	0.000	0.071	2.017	2.985	0.000	0.253	1.346	1.322	0.006	0.001	0.000	0.001
227-1	0.000	0.069	1.999	2.995	0.000	0.313	1.312	1.302	0.006	0.000	0.001	0.000
227-1	0.001	0.067	2.010	2.990	0.000	0.335	1.275	1.316	0.006	0.000	0.000	0.000
227-1	0.000	0.069	2.016	2.984	0.001	0.345	1.241	1.342	0.005	0.001	0.000	0.000
227-1	0.001	0.073	2.014	2.987	0.001	0.362	1.214	1.343	0.005	0.000	0.000	0.000
227-1	0.000	0.068	2.015	2.984	0.000	0.368	1.235	1.328	0.004	0.001	0.000	0.000
227-1	0.001	0.059	2.012	2.989	0.001	0.342	1.321	1.267	0.005	0.001	0.000	0.002
84-1	0.002	0.162	2.016	2.975	0.003	0.077	0.474	2.297	0.004	0.001	0.000	0.002
84-1	0.006	0.202	2.012	2.976	0.001	0.068	0.425	2.326	0.000	0.001	0.000	0.003
84-1	0.006	0.240	2.014	2.975	0.000	0.078	0.388	2.307	0.000	0.001	0.000	0.007
84-1	0.004	0.244	2.004	2.980	0.000	0.086	0.383	2.307	0.000	0.001	0.000	0.007
84-1	0.006	0.250	2.005	2.977	0.000	0.088	0.379	2.304	0.001	0.000	0.000	0.007
84-1	0.012	0.255	2.004	2.975	0.001	0.091	0.376	2.301	0.001	0.001	0.000	0.008
84-1	0.006	0.256	2.009	2.975	0.001	0.090	0.371	2.304	0.001	0.000	0.000	0.006

SAMPLE	Na	Mg	Al	Si	K	Ca	Mn	Fe	Ti	Cr	Zr	Y
84-1	0.009	0.261	2.010	2.974	0.000	0.089	0.372	2.296	0.001	0.001	0.000	0.007
84-1	0.008	0.258	2.016	2.967	0.000	0.087	0.363	2.316	0.002	0.000	0.000	0.006
84-1	0.007	0.262	2.008	2.966	0.000	0.089	0.369	2.322	0.000	0.000	0.000	0.006
84-1	0.012	0.261	2.025	2.960	0.000	0.089	0.364	2.309	0.001	0.001	0.000	0.007
84-1	0.012	0.263	2.021	2.958	0.001	0.096	0.366	2.303	0.002	0.002	0.000	0.008
84-1	0.009	0.261	2.020	2.968	0.000	0.094	0.369	2.289	0.002	0.000	0.000	0.007
84-1	0.015	0.263	2.017	2.972	0.000	0.088	0.362	2.299	0.002	0.000	0.000	0.005
84-1	0.008	0.262	2.012	2.973	0.000	0.089	0.365	2.301	0.002	0.000	0.000	0.006
84-1	0.015	0.255	2.009	2.979	0.001	0.088	0.363	2.304	0.000	0.001	0.000	0.006
84-1	0.008	0.260	2.008	2.976	0.000	0.088	0.364	2.309	0.000	0.001	0.000	0.007
84-1	0.008	0.256	2.009	2.981	0.001	0.083	0.368	2.301	0.000	0.002	0.000	0.005
84-1	0.008	0.250	2.015	2.974	0.000	0.082	0.377	2.306	0.000	0.001	0.000	0.006
84-1	0.005	0.245	2.016	2.980	0.000	0.072	0.380	2.308	0.000	0.001	0.000	0.005
137-1	0.004	0.198	2.023	2.985	0.003	0.103	0.287	2.402	0.001	0.000	0.000	0.000
137-1	0.007	0.245	2.022	2.982	0.001	0.114	0.437	2.199	0.000	0.000	0.000	0.003
137-1	0.010	0.227	2.019	2.979	0.001	0.122	0.522	2.116	0.002	0.001	0.000	0.011
137-1	0.010	0.219	2.023	2.979	0.001	0.133	0.555	2.071	0.002	0.001	0.000	0.013
137-1	0.009	0.210	2.025	2.970	0.001	0.141	0.582	2.056	0.003	0.001	0.000	0.014
137-1	0.008	0.205	2.025	2.975	0.000	0.141	0.605	2.036	0.001	0.000	0.000	0.013

SAMPLE	Na	Mg	Al	Si	K	Ca	Mn	Fe	Ti	Cr	Zr	Y
137-1	0.009	0.198	2.020	2.976	0.001	0.136	0.627	2.022	0.004	0.001	0.000	0.015
137-1	0.009	0.196	2.008	2.983	0.000	0.140	0.644	1.996	0.009	0.000	0.000	0.016
137-1	0.011	0.196	2.014	2.981	0.001	0.147	0.654	1.987	0.002	0.000	0.000	0.015
137-1	0.009	0.195	2.009	2.985	0.000	0.150	0.657	1.978	0.003	0.000	0.000	0.017
137-1	0.012	0.194	2.018	2.977	0.001	0.155	0.658	1.980	0.002	0.000	0.000	0.014
137-1	0.014	0.195	2.015	2.975	0.001	0.152	0.661	1.986	0.002	0.000	0.000	0.015
137-1	0.009	0.195	2.018	2.977	0.001	0.142	0.644	2.003	0.003	0.000	0.000	0.015
137-1	0.013	0.198	2.017	2.995	0.001	0.136	0.626	1.985	0.005	0.000	0.000	0.015
137-1	0.009	0.211	2.005	2.980	0.002	0.138	0.597	2.054	0.002	0.001	0.000	0.014
137-1	0.011	0.218	1.999	2.994	0.001	0.136	0.568	2.062	0.003	0.000	0.000	0.012
137-1	0.008	0.224	2.009	2.990	0.001	0.128	0.534	2.100	0.000	0.000	0.000	0.010
137-1	0.010	0.234	2.009	2.980	0.001	0.115	0.509	2.146	0.002	0.000	0.000	0.008
137-1	0.004	0.258	2.007	2.984	0.000	0.128	0.386	2.242	0.002	0.000	0.000	0.001
137-1	0.006	0.229	2.016	2.987	0.002	0.115	0.272	2.380	0.001	0.000	0.000	0.000

Appendix II

Table of end-member compositions for each point in garnets for all samples

Sample no.	Points	Almandine	Spessartine	Pyrope	Grossular
217-1	1	0.603	0.290	0.035	0.070
217-1	2	0.583	0.294	0.034	0.078
217-1	3	0.570	0.307	0.032	0.090
217-1	4	0.549	0.327	0.030	0.092
217-1	5	0.505	0.354	0.026	0.107
217-1	6	0.498	0.358	0.026	0.115
217-1	7	0.511	0.369	0.028	0.090
217-1	8	0.510	0.368	0.027	0.093
217-1	9	0.496	0.372	0.026	0.105
217-1	10	0.495	0.376	0.026	0.101
217-1	11	0.496	0.377	0.026	0.100
217-1	12	0.502	0.380	0.026	0.091
217-1	13	0.505	0.372	0.027	0.096
217-1	14	0.499	0.367	0.026	0.106
217-1	15	0.510	0.368	0.027	0.092
217-1	16	0.502	0.355	0.026	0.115
217-1	17	0.516	0.349	0.026	0.107
217-1	18	0.540	0.336	0.028	0.094
217-1	19	0.576	0.313	0.031	0.077
217-1	20	0.606	0.292	0.035	0.065
262-2 grt1	1	0.542	0.328	0.038	0.093
262-2 grt1	2	0.511	0.339	0.035	0.113
262-2 grt1	3	0.476	0.359	0.030	0.135
262-2 grt1	4	0.435	0.398	0.024	0.143
262-2 grt1	5	0.463	0.402	0.026	0.100
262-2 grt1	6	0.475	0.408	0.028	0.088
262-2 grt1	7	0.468	0.400	0.026	0.105
262-2 grt1	8	0.461	0.419	0.028	0.091
262-2 grt1	9	0.456	0.429	0.027	0.087
262-2 grt1	10	0.450	0.434	0.029	0.085
262-2 grt1	11	0.450	0.428	0.026	0.096
262-2 grt1	12	0.455	0.418	0.026	0.101
262-2 grt1	13	0.460	0.414	0.026	0.100
262-2 grt1	14	0.473	0.400	0.028	0.098
262-2 grt1	15	0.475	0.407	0.026	0.092
262-2 grt1	16	0.435	0.397	0.023	0.144
262-2 grt1	17	0.442	0.389	0.024	0.145
262-2 grt1	18	0.462	0.365	0.028	0.146
262-2 grt1	19	0.489	0.344	0.032	0.135
262-2 grt1	20	0.534	0.327	0.037	0.101
262-2 grt2	1	0.528	0.343	0.035	0.093
262-2 grt2	2	0.496	0.349	0.033	0.122
262-2 grt2	3	0.470	0.380	0.035	0.115
262-2 grt2	4	0.477	0.403	0.031	0.089
262-2 grt2	5	0.476	0.406	0.030	0.087

Sample no.	Points	Almandine	Spessartine	Pyrope	Grossular
262-2 grt2	6	0.478	0.417	0.022	0.080
262-2 grt2	7	0.498	0.404	0.020	0.077
262-2 grt2	8	0.478	0.420	0.020	0.080
262-2 grt2	9	0.484	0.410	0.025	0.079
262-2 grt2	10	0.485	0.410	0.024	0.080
262-2 grt2	11	0.485	0.409	0.025	0.080
262-2 grt2	12	0.482	0.405	0.026	0.086
262-2 grt2	13	0.482	0.404	0.030	0.083
262-2 grt2	14	0.484	0.403	0.031	0.080
262-2 grt2	15	0.480	0.402	0.030	0.086
262-2 grt2	16	0.476	0.391	0.033	0.098
262-2 grt2	17	0.478	0.362	0.032	0.126
262-2 grt2	18	0.489	0.350	0.035	0.125
262-2 grt2	19	0.524	0.345	0.034	0.096
211-1	1	0.729	0.100	0.052	0.117
211-1	2	0.593	0.238	0.048	0.122
211-1	3	0.540	0.301	0.040	0.119
211-1	4	0.529	0.322	0.037	0.112
211-1	5	0.518	0.335	0.036	0.112
211-1	6	0.513	0.346	0.035	0.106
211-1	7	0.507	0.352	0.039	0.103
211-1	8	0.498	0.352	0.042	0.108
211-1	9	0.505	0.350	0.039	0.105
211-1	10	0.505	0.351	0.037	0.105
211-1	11	0.508	0.351	0.037	0.104
211-1	12	0.507	0.347	0.038	0.109
211-1	13	0.507	0.347	0.039	0.107
211-1	14	0.506	0.342	0.040	0.113
211-1	15	0.516	0.324	0.040	0.120
211-1	16	0.528	0.316	0.041	0.115
211-1	17	0.536	0.295	0.042	0.126
211-1	18	0.559	0.254	0.044	0.143
211-1	19	0.612	0.193	0.052	0.142
211-1	20	0.701	0.162	0.067	0.070
211-1	21	0.745	0.132	0.072	0.050
211-1	22	0.780	0.102	0.073	0.043
208-2	1	0.825	0.081	0.072	0.021
208-2	2	0.783	0.102	0.089	0.027
208-2	3	0.746	0.137	0.081	0.036
208-2	4	0.702	0.172	0.072	0.054
208-2	5	0.651	0.210	0.061	0.078
208-2	6	0.613	0.244	0.054	0.090
208-2	7	0.580	0.276	0.047	0.096
208-2	8	0.548	0.309	0.040	0.103
208-2	9	0.524	0.335	0.035	0.106

Sample no.	Points	Almandine	Spessartine	Pyrope	Grossular
208-2	10	0.521	0.348	0.037	0.091
208-2	11	0.522	0.348	0.037	0.089
208-2	12	0.520	0.350	0.036	0.092
208-2	13	0.520	0.348	0.036	0.094
208-2	14	0.520	0.345	0.036	0.098
208-2	15	0.542	0.316	0.039	0.103
208-2	16	0.576	0.280	0.046	0.098
208-2	17	0.603	0.255	0.051	0.091
208-2	18	0.670	0.200	0.065	0.065
208-2	19	0.728	0.158	0.078	0.037
208-2	20	0.779	0.109	0.086	0.026
208-2	21	0.803	0.088	0.086	0.022
208-2	22	0.821	0.080	0.077	0.020
199-1	1	0.655	0.232	0.055	0.056
199-1	2	0.649	0.218	0.068	0.063
199-1	3	0.647	0.219	0.064	0.068
199-1	4	0.647	0.222	0.060	0.070
199-1	5	0.647	0.228	0.052	0.071
199-1	6	0.646	0.225	0.059	0.070
199-1	7	0.652	0.231	0.049	0.067
199-1	8	0.657	0.239	0.046	0.056
199-1	9	0.654	0.246	0.043	0.056
199-1	10	0.651	0.231	0.049	0.068
199-1	11	0.654	0.228	0.053	0.064
199-1	12	0.645	0.232	0.048	0.074
199-1	13	0.645	0.220	0.062	0.073
199-1	14	0.638	0.219	0.060	0.083
199-1	15	0.650	0.226	0.056	0.068
199-1	16	0.644	0.218	0.061	0.076
199-1	17	0.645	0.222	0.061	0.071
199-1	18	0.654	0.232	0.051	0.062
199-1	19	0.646	0.224	0.060	0.070
199-1	20	0.642	0.217	0.065	0.075
199-1	21	0.654	0.214	0.070	0.060
199-1	22	0.653	0.222	0.063	0.060
227-1	1	0.436	0.427	0.021	0.116
227-1	2	0.451	0.395	0.023	0.130
227-1	3	0.444	0.416	0.022	0.118
227-1	4	0.441	0.427	0.023	0.106
227-1	5	0.437	0.436	0.022	0.104
227-1	6	0.440	0.449	0.021	0.088
227-1	7	0.440	0.456	0.022	0.082
227-1	8	0.424	0.446	0.023	0.083
227-1	9	0.437	0.456	0.027	0.080
227-1	10	0.434	0.460	0.024	0.081

Sample no.	Points	Almandine	Spessartine	Pyrope	Grossular
227-1	11	0.433	0.460	0.024	0.083
227-1	12	0.434	0.458	0.023	0.084
227-1	13	0.436	0.455	0.023	0.084
227-1	14	0.442	0.450	0.024	0.085
227-1	15	0.434	0.438	0.023	0.104
227-1	16	0.440	0.426	0.022	0.112
227-1	17	0.448	0.414	0.023	0.115
227-1	18	0.449	0.406	0.024	0.121
227-1	19	0.443	0.412	0.023	0.123
227-1	20	0.424	0.442	0.020	0.114
84-1	1	0.763	0.157	0.054	0.025
84-1	2	0.769	0.141	0.067	0.022
84-1	3	0.764	0.129	0.079	0.026
84-1	4	0.763	0.127	0.081	0.029
84-1	5	0.761	0.125	0.083	0.029
84-1	6	0.758	0.124	0.084	0.030
84-1	7	0.761	0.123	0.084	0.030
84-1	8	0.758	0.123	0.086	0.030
84-1	9	0.764	0.120	0.085	0.029
84-1	10	0.761	0.121	0.086	0.029
84-1	11	0.761	0.120	0.086	0.029
84-1	12	0.758	0.120	0.086	0.031
84-1	13	0.758	0.122	0.086	0.031
84-1	14	0.759	0.120	0.087	0.029
84-1	15	0.761	0.121	0.087	0.029
84-1	16	0.762	0.120	0.084	0.029
84-1	17	0.762	0.120	0.086	0.029
84-1	18	0.763	0.122	0.085	0.028
84-1	19	0.763	0.125	0.083	0.027
84-1	20	0.767	0.126	0.081	0.024
137-1	1	0.802	0.096	0.066	0.034
137-1	2	0.733	0.146	0.082	0.038
137-1	3	0.706	0.174	0.076	0.041
137-1	4	0.693	0.186	0.073	0.044
137-1	5	0.686	0.194	0.070	0.047
137-1	6	0.680	0.202	0.068	0.047
137-1	7	0.676	0.209	0.066	0.045
137-1	8	0.669	0.216	0.066	0.047
137-1	9	0.664	0.218	0.065	0.049
137-1	10	0.662	0.220	0.065	0.050
137-1	11	0.660	0.219	0.065	0.052
137-1	12	0.660	0.220	0.065	0.051
137-1	13	0.669	0.215	0.065	0.047
137-1	14	0.671	0.212	0.067	0.046
137-1	15	0.683	0.198	0.070	0.046

Sample no.	Points	Almandine	Spessartine	Pyrope	Grossular
137-1	16	0.688	0.190	0.073	0.045
137-1	17	0.701	0.178	0.075	0.043
137-1	18	0.712	0.169	0.078	0.038
137-1	19	0.743	0.128	0.086	0.042
137-1	20	0.793	0.091	0.076	0.038

Appendix III

Diffusivities for garnets from different metamorphic grade zones and diffusive distance in 45 Ma

Sample no.	P(Pa)	T(K)	End-members	X	a_0	$logfo_2$	$logfo_2^{gr}$	$D(m^2/s)$	logD	x(um)
227-1	3.80E+08	773.15	alm	0.451	1.16E-09	-24.30	-23.30	2.75E-25	-24.56	39.51
			spss	0.395				5.43E-27	-26.26	5.55
			py	0.023				1.12E-23	-22.95	252.69
			grs	0.130				3.77E-32	-31.42	0.01
262-2 grt1	4.50E+08	790.15	alm	0.534	1.16E-09	-23.30	-22.00	1.84E-25	-24.73	32.36
			spss	0.327				3.53E-27	-26.45	4.47
			py	0.037				8.18E-24	-23.09	215.55
			grs	0.101				2.11E-32	-31.68	0.01
262-2 grt2	3.80E+09	778.15	alm	0.534	1.16E-09	-23.60	-22.60	9.74E-29	-28.01	0.74
			spss	0.327				1.44E-29	-28.84	0.29
			py	0.037				6.08E-26	-25.22	18.58
			grs	0.101				8.56E-35	-34.07	0.00
217-1	3.00E+08	794.15	alm	0.603	1.15E-09	-23.20	-22.10	9.65E-26	-25.02	23.41
			spss	0.290				1.55E-27	-26.81	2.97
			py	0.035				4.24E-24	-23.37	155.22
			grs	0.070				8.75E-33	-32.06	0.01
211-1	4.50E+08	849.15	alm	0.780	1.15E-09	-21.50	-20.80	5.20E-25	-24.28	54.31
			spss	0.102				8.49E-27	-26.07	6.94
			py	0.073				2.22E-23	-22.65	355.25
			grs	0.043				3.34E-32	-31.48	0.01
208-2	4.00E+08	897.15	alm	0.821	1.15E-09	-22.00	-21.00	1.56E-24	-23.81	94.24
			spss	0.080				2.31E-26	-25.64	11.44
			py	0.077				5.97E-23	-22.22	582.31
			grs	0.020				6.84E-32	-31.17	0.02
137-1	5.50E+08	873.15	alm	0.802	1.15E-09	-20.80	-20.00	8.47E-25	-24.07	69.36
			spss	0.096				1.42E-26	-25.85	8.97
			py	0.066				3.68E-23	-22.43	456.90
			grs	0.034				4.83E-32	-31.32	0.02
199-1	4.50E+08	808.15	alm	0.653	1.16E-09	-22.50	-21.80	2.15E-25	-24.67	34.91
			spss	0.222				3.82E-27	-26.42	4.65
			py	0.063				9.73E-24	-23.01	235.06
			grs	0.060				1.98E-32	-31.70	0.01
84-1	5.00E+08	923.15	alm	0.769	1.15E-09	-19.30	-18.80	5.76E-24	-23.24	180.84
			spss	0.141				9.04E-26	-25.04	22.65
			py	0.067				2.10E-22	-21.68	1092.17
			grs	0.022				2.37E-31	-30.62	0.04

Appendix IV

Diffusive time for each garnet calculated by $x = 2\sqrt{Dt}$. D is the diffusion coefficient calculated and X is the widest rim measured according to zoning map for each garnet.

Sample no.	Endmembers	X'(um)	t(mil year)
227-1	alm	155.56	6.98E+02
	spss		3.53E+04
	py		1.71E+01
	grs		5.09E+09
262-2 grt1	alm	60.54	1.58E+02
	spss		8.24E+03
	py		3.55E+00
	grs		1.37E+09
262-2 grt2	alm	35.79	1.04E+05
	spss		7.07E+05
	py		1.67E+02
	grs		1.19E+11
217-1	alm	83.82	5.77E+02
	spss		3.59E+04
	py		1.31E+01
	grs		6.36E+09
211-1	alm	106.67	1.74E+02
	spss		1.06E+04
	py		4.06E+00
	grs		2.70E+09
208-2	alm	154.29	1.21E+02
	spss		8.19E+03
	py		3.16E+00
	grs		2.76E+09
137-1	alm	170	2.70E+02
	spss		1.62E+04
	py		6.23E+00
	grs		4.74E+09
199-1	alm	66.67	1.64E+02
	spss		9.24E+03
	py		3.62E+00
	grs		1.78E+09
84-1	alm	46	2.91E+00
	spss		1.86E+02
	py		7.98E-02
	grs		7.07E+07